J. Fluid Mech. (2004), *vol.* 520, *pp.* 51–82.
DOI: 10.1017/S0022112004001594 Printed in the United Kingdom

Numerical solution of the Navier–Stokes equations for the flow in a cylinder cascade

By J. S. B. GAJJAR AND NABILA A. AZZAM

Mathematics Department, University of Manchester, Manchester M13 9PL, UK

(Received 5 March 2003 and in revised form 12 July 2004)

A numerical study of the steady, two-dimensional incompressible flow past a cascade of circular cylinders is presented. The Navier–Stokes equations are written in terms of the streamfunction and vorticity and solved using a novel numerical technique based on using the Chebychev collocation method in one direction and high-order finite differences in the other direction. A direct solver combined with Newton–Raphson linearization is used to solve the discrete equations. Steady flow solutions have been obtained for large Reynolds numbers, far higher than those obtained previously, and for varying gap widths between the cylinders. Three distinct types of solutions, dependent on the gap width, have been found. Comparisons with theoretical predictions for various flow quantities show good agreement, especially for the narrow gap width case. However, existing theories are unable to explain the solution properties which exist for intermediate gap widths.

1. Introduction

The solution of the Navier–Stokes equations for large Reynolds number is an area of considerable interest to theoreticians as well as numerical analysts. Notwithstanding the numerous techniques and algorithms which have been developed, obtaining an accurate solution of the equations for large Reynolds number poses considerable difficulty because of the various scales and thin regions which need to be resolved. One classical problem which exhibits such difficulties is the computation of the steady incompressible fluid flow past a circular cylinder. For the theoretician the challenge is to obtain a description of the flow structure in the limit of the Reynolds number becoming large using asymptotic methods to obtain insight into high Reynolds number flow past a general bluff body. For the numerical analyst the resolution of the important features of the flow provides one of the challenges in tacking the full problem.

In spite of the many numerical methods and calculations on flow past a circular cylinder, accurate results have been reported only for Reynolds number ($R = Ud/v$, where U is the uniform speed relative to the cylinder at large distance, d the diameter of the cylinder and v the kinematic viscosity of the fluid) up to about 800, see Fornberg (1991).

One important aspect of the steady flow problem is the correct description of the flow features for large Reynolds numbers. This is an area which has aroused considerable controversy. We note that the real flow past a cylinder becomes unsteady and turbulent at fairly low Reynolds numbers and therefore the motivation of computing the steady flow requires further explanation. It can be argued that an accurate solution of the steady flow is needed before the departure from the steady state can be described, and this is one of the reasons for computing the steady flow. Another

reason is that the bulk of the asymptotic theory for this and related problems is based on a steady flow description. Finally the techniques which have been developed here may be applied to investigate other flows where the steady flow is of primary interest.

Concerning the theory of steady flow past a circular cylinder, it is now generally accepted that as the Reynolds number is increased, the fluid flow separates from the surface of the cylinder and an eddy forms behind the cylinder. One of the principal focuses of attention of many of the theoretical studies was to try to obtain the description of the separation as well as the eddy structure in the limit of the Reynolds number being asymptotically large. An excellent review of much of this work has been given by Chernyshenko (1998). The review describes the complicated flow structure which arises in the steady flow past bluff bodies and in particular the flow past a circular cylinder at large Reynolds numbers. It is worth highlighting the different flow feature on the body scale as well as on the eddy scale which need to be taken into account when doing numerical computations. First, on the body scale the adverse pressure gradient on the forward part of the body leads to boundary layer separation. In fact locally near the point of separation the pressure gradient becomes singular like $O(R^{-1/32}(s_0 - s)^{-1/2})$ where s is the distance along the body surface and s_0 the point of separation. This behaviour ensures that the boundary layer separates smoothly from the body, see Smith (1979). The inviscid flow locally near the separation point is described by the Kirchhoff (1869) free-streamline theory. Next, on the eddy scale, the dominant feature is the presence of a large eddy comprising a pair of closed streamline regions of constant vorticity. On the eddy scale the cylinder appears as a point. It is the description of the eddy features which has raised most controversy.

Batchelor (1956), was one of the first to try to describe the eddy features. He suggested that the eddy dimensions remain $O(1)$ in the limit that $R \to \infty$. Acrivos *et al.* (1965) made another suggestion that the eddy length grows linearly with the Reynolds number whilst the eddy width remains $O(1)$. This was motivated by their experimental results but some of the experiments were conducted with a splitter plate behind the cylinder. Both of these suggestions have been found to lead to inconsistencies in the more detailed theoretical investigations of the flow.

Smith (1979) and Sychev (1967, 1982) studied the incompressible flow past a bluff body from the theoretical perspective. They developed an asymptotic theory which is based on an extension of Kirchhoff's (1869) free-streamline theory. The paper by Smith (1979) gives the most detailed theoretical description of the flow field, as well as historical account of previous work on the problem. Smith (1979) suggested that the eddy length grows linearly with the Reynolds number whilst the eddy width grows like $O(R^{1/2})$.

Fornberg, in a series of papers starting with Fornberg (1980), was one of the first to obtain an accurate numerical solution to the problem of high Reynolds number flow past an isolated cylinder. In Fornberg (1980) he managed to obtain solutions for Reynolds number up to 300. The eddy dimensions were found to increase linearly with Reynolds number, consistent with the Smith (1979) theory. Following this Fornberg (1983) showed that for Reynolds number greater than 300 the eddy grew linearly in both dimensions as the Reynolds number increased. These additional results contradicted the earlier suggestion that the eddy ceased to grow after $R > 300$, see Fornberg (1985). In this latter work it was argued that extreme care needs to be exercised in the implementation of the boundary conditions, the choice of the numerical algorithm, grid independence studies and so on, and that much of the earlier numerical work by others was suspect on these grounds. Fornberg (1985) showed that the wake bubble has eddy length $O(R)$, with width $O(R^{1/2})$ up to about

$R = 300$, and thereafter both the eddy length and eddy width increase linearly with Reynolds number.

The paper by Taganov (1968) is one of the earliest in which a theory of the eddy flow with eddy width and eddy length increasing with Reynolds numbers was proposed. Later Sadovskii (1970) made calculations based on this theory and obtained results for the one-parameter family of potential flow vortices, now called Sadovskii vortices. Following Fornberg (1985), Peregrine (1985) and Smith (1985*b*) also put forward a revised theory based on the Sadovskii model in which the eddy dimensions grew linearly with Reynolds number. However, there were many aspects of the theory which were left unsolved. Later Chernyshenko (1988), and Chernyshenko & Castro (1996) solved a number of these outstanding technical problems and gave definite predictions for the behaviours of some of the global properties such as drag, eddy vorticity and so on, as a function of the Reynolds number.

Subsequently, the work on cylinder flows was also extended to other geometries such as the flow past flat plates inclined normally to the oncoming stream. Fornberg (1991) extended his calculation to obtain an accurate solution to the steady Navier–Stokes equations for flow past a cascade of circular cylinders. His numerical work showed that for large gap widths between the cylinders, the eddy behind each cylinder was growing in size with increasing Reynolds numbers, in line with theoretical predictions by Chernyshenko & Castro (1996). On the other hand a major change in the solution properties occurs for small and moderate gap widths. For very small gap widths the eddy is long and slender with the width remaining constant with increasing Reynolds numbers. The solution features here are similar to that postulated by Acrivos *et al.* (1965). Our numerical calculations show that for moderate gap widths, the eddy is long and slender but there is a dramatic change in properties near reattachment where the features for a large gap width seem to emerge.

A study of the full Navier–Stokes equations in the related flat-plate cascade geometry in Ingham, Tang & Morton (1990), Natarajan, Fornberg & Acrivos (1993) again confirmed the existence of a qualitatively new regime of flow solution for gap widths above a certain critical value. For large gap widths the solution properties are qualitatively similar to that obtained in Fornberg (1991) for a row of cylinders. They suggested that the flow behaviour might be generic for any symmetric bluff body and also suggested a fundamental difference between the case where the vorticity distribution in the initial separating flow is determined in the attached boundary layer at the front of the bluff body, and the case studied by Milos & Acrivos (1987) where the vorticity distribution is specified as part of the boundary condition for the inlet flow to the cascade. Recently Castro (2002) has extended earlier work for the flow past a cascade of flat plates to stratified fluids.

The flow we consider here is that past a cascade of circular cylinders placed in a uniform stream. In addition to the Reynolds number, this introduces an additional parameter, namely the gap width W between the cylinders. The asymptotic theory for this so-called cascade flow is less well developed than that for the isolated body case. Nevertheless some results are available in the limit $R \to \infty$ with $W = O(R)$. The structure is similar to that for the isolated cylinder case and is described by Chernyshenko & Castro (1993). For $W = O(1)$ a numerical treatment is necessary. Some results have also been predicted for the case $W/R \to 0$, $W \gg 1$, $R \gg 1$.

One of the objectives of the current work is to present a somewhat unconventional but robust technique for the solution of the steady Navier–Stokes equations and other similar equations. The numerical algorithm used involves high-order finite differences in one direction combined with spectral collocation in the other direction. Another

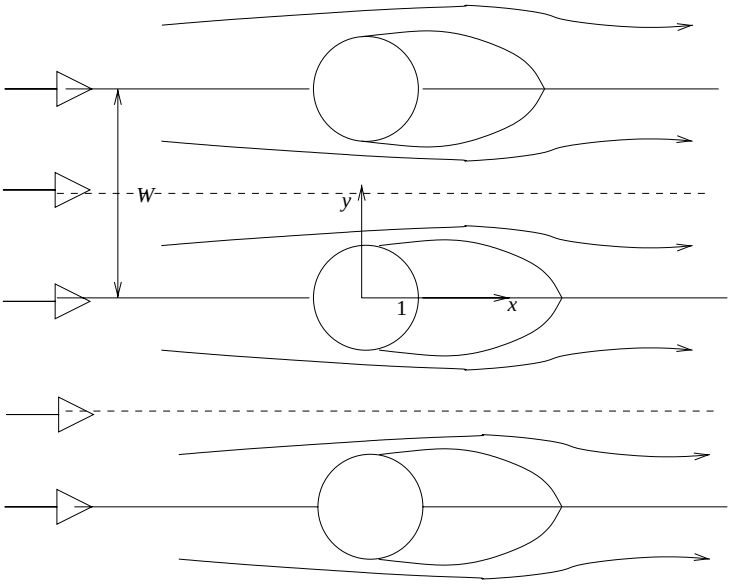

FIGURE 1. Sketch of flow past a cascade of circular cylinders.

objective of this work is to present some new results obtained using the technique for the flow past a cascade of circular cylinders at large Reynolds numbers.

In §§2–5 we discuss the formulation of the problem and the numerical techniques used. The results obtained using the method are discussed in §6 and finally we finish with some conclusions.

2. Problem formulation

The cascade is assumed to consist of an infinite number of circular cylinders of non-dimensional radius unity, placed in a uniform stream with the centres of the cylinders a non-dimensional width W apart, see figure 1. At large distances from the cascade the fluid is assumed to be moving with constant speed U in the positive x-direction and because of the symmetry in the y-direction we need consider only two-dimensional flow in the region $0 \leqslant y \leqslant W/2$.

Consider the Navier–Stokes equations in vorticity (ω)–streamfunction (ψ) formulation for a cylinder of non-dimensional radius 1 and Reynolds number R (based on the cylinder diameter), written as

$$\psi_y \omega_x - \psi_x \omega_y = \frac{2}{R} \nabla^2 \omega, \tag{2.1}$$

$$\nabla^2 \psi + \omega = 0. \tag{2.2}$$

Here $R = Ud/v$, where U is the uniform speed relative to the cylinder at large distances from the cylinder, d the diameter of the cylinder and v the kinematic viscosity of the fluid.

Because of symmetry we can restrict attention to the flow region shown in figure 2. The equations have to be solved subject to boundary conditions of no slip on the body surface. In addition, on the two primary symmetry lines $y = 0$ and $y = W/2$, the conditions are $\psi = \omega = 0$ on $y = 0$, $|x| > 1$ and $\psi = W/2$, $\omega = 0$ on $y = W/2$. Finally, $\psi \to y$ and $\omega = 0$ holds as $x \to \pm\infty$.

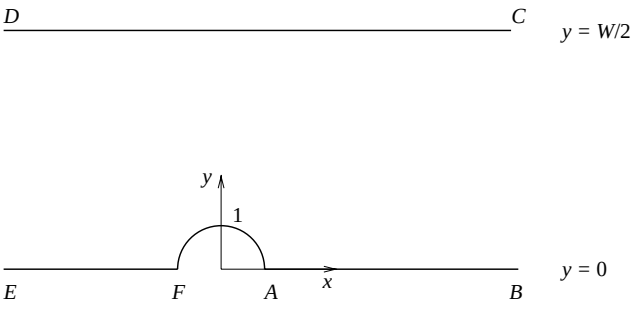

FIGURE 2. Sketch of the physical domain.

The equations together with the boundary conditions have to be solved to obtain the streamfunction ψ and vorticity ω for various values of the Reynolds number R and the additional parameter W.

The equations are solved first by transforming the physical domain in the (x, y)-plane to a strip in the (ξ, η)-domain. A conformal mapping is used similar to that described by Fornberg (1991).

A mixed finite-difference spectral method is used to solve the equations, with fourth-order-finite differences in the ξ-direction and Chebychev collocation in the η-direction. This is very different from the second-order finite difference method used by Fornberg (1991).

3. Mapping transformation

A conformal mapping is used to transform the basic computational domain to a rectangular region where the mesh generation is greatly simplified. After such mapping from a complex $(X = x + \mathrm{i}y)$ plane to a $(Z = \xi + \mathrm{i}\eta)$ plane an additional factor J is introduced in one of the governing equations, which become

$$\frac{\partial^2\omega}{\partial\xi^2} + \frac{\partial^2\omega}{\partial\eta^2} + \frac{1}{2}R\left\{\frac{\partial\psi}{\partial\xi}\frac{\partial\omega}{\partial\eta} - \frac{\partial\psi}{\partial\eta}\frac{\partial\omega}{\partial\xi}\right\} = 0, \tag{3.1}$$

$$\left\{\frac{\partial^2\psi}{\partial\xi^2} + \frac{\partial^2\psi}{\partial\eta^2}\right\} J + \omega = 0, \tag{3.2}$$

where $J = |\mathrm{d}Z/\mathrm{d}X|$ is the Jacobian of the transformation.

The mapping we use takes the original computational domain ABCDEF in the X-plane, see figure 2, to a strip $A'B'C'D'E'F'$ in the Z-plane as indicated in figure 3. The transformation is the same as in Fornberg (1991) with $T = (\pi/W)\coth(\pi Z/W)$, and given by letting

$$X = \frac{V}{W}\left\{Z + \sum_{k=1}^{\infty}\alpha_k T^{2k-1}\right\}. \tag{3.3}$$

Here V and $\{\alpha_i\}$ are real constants and chosen such that $X = \mathrm{e}^{\mathrm{i}\theta}$ maps to $\eta = 0$ and $-2 \leqslant \xi \leqslant 2$ for $0 \leqslant \theta \leqslant \pi$. Also $y = W/2$ is mapped to $\eta = V/2$. The value of V can be obtained by putting $X = 1$ and setting $Z = 2$. The coefficients α_k can be calculated as in Fornberg (1991). Table 1 gives values for W, V and $\{\alpha_i\}$ that we calculated by using the symbolic package Mathematica.

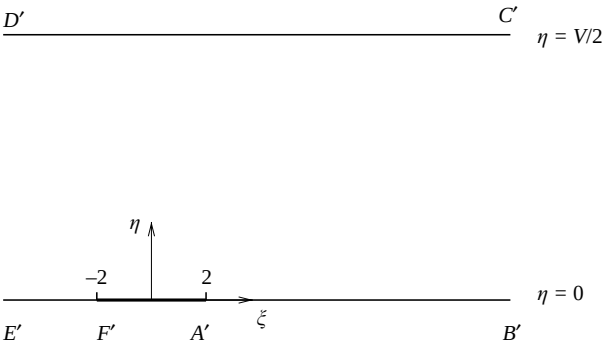

FIGURE 3. Sketch of the transformed domain.

W	5	10	20
V	4.356406392635564	9.67308621426570	19.8357743123441
α_1	1.1531763706116489	1.0340400782648907	1.0082932136650135
α_2	−0.0040942260731489	−0.0002241793310169	−0.000013642557745
α_3	0.0001559958018689	$2.108785214 \times 10^{-6}$	3.206019×10^{-8}
α_4	$-6.23943862 \times 10^{-6}$	$-2.08276999 \times 10^{-8}$	-7.91088×10^{-11}
α_5	2.5171939×10^{-7}	$2.0778269 \times 10^{-10}$	1.972×10^{-13}
α_6	$-9.5370049 \times 10^{-9}$	-2.0689×10^{-12}	-4.9×10^{-16}
W	50	100	1000
V	49.93421992520	99.967103482	999.9967
α_1	1.0013176826219767	1.0003290951026844	1.0000032898789570
α_2	$-3.4680066 \times 10^{-7}$	-2.165360×10^{-8}	-2×10^{-12}
α_3	1.30×10^{-10}	$0. \times 10^{-12}$	-0×10^{-8}
α_4	-5.15×10^{-14}	-2.0×10^{-16}	-2.0×10^{-24}
α_5	$2. \times 10^{-17}$	$2. \times 10^{-20}$	2×10^{-30}
α_6	$-8. \times 10^{-21}$	$-2. \times 10^{-24}$	-2×10^{-36}

TABLE 1. The values of α for $W = 5$, 10, 20, 50, 100 and 1000.

The mapping described above takes a region in the X-plane and transforms it to a strip in the Z-plane, see figures 2 and 3 subject to the following boundary conditions:

On the line $E'F'$ $(\xi < -2, \eta = 0)$ $\psi = 0, \omega = 0.$
On $A'B'$: $(\xi > 2, \eta = 0)$ $\psi = 0, \omega = 0.$
On $F'A'$: $(|\xi| \leqslant 2, \eta = 0)$ $\psi = 0, \psi_\eta = 0.$
On $E'D'$: $(\xi = -\infty)$ $\psi = \eta, \omega = 0, \psi_\xi = 0.$
On $B'C'$: $(\xi = \infty)$ $\psi = \eta, \omega = 0, \psi_\xi = 0.$
On $D'C'$: $(\eta = V/2)$ $\psi = W/2, \ \omega = 0.$

Since the resolution requirements are different in different parts of this region, we consider a further transformation in the ξ-direction such that $\xi = g(\tau)$ is used where $g(\tau)$ is a combination of cubic and quintic splines (see figure 4). We use an equi-spaced grid in the τ-plane. The mapping between the Z-plane and this plane consists of independent grid stretching described as follows. For $\tau < -2$

$$g(\tau) = a_0 + a_1(\tau + 2) + a_2(\tau + 2)^2 + a_3(\tau + 2)^3 \tag{3.4}$$

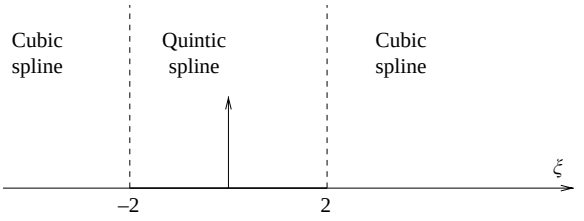

FIGURE 4. Sketch of the transformed domain.

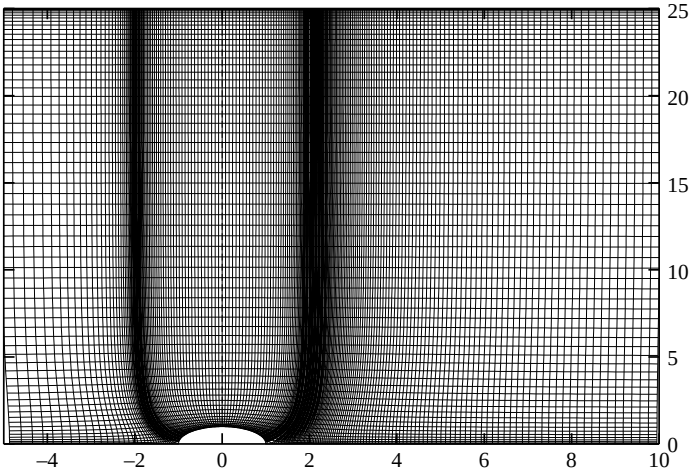

FIGURE 5. Grid lines in the X-plane.

and the a_i are calculated subject to the conditions $g(-2) = -2$, $g_\tau(-2) = 0.3$, $g_{\tau\tau}(-2) = 0$ and $\xi(-3) = -3$.

For $\tau > 2$, we let

$$g(\tau) = b_0 + b_1(\tau - 2) + b_2(\tau - 2)^2 + b_3(\tau - 2)^3 \tag{3.5}$$

and the conditions used here to find b_i are $g(2) = 2$, $g_\tau(2) = 0.3$, $g_{\tau\tau}(2) = 0$ and $g(21) = 300$.

When $-2 < \tau < 2$

$$g(\tau) = c_0 + c_1\tau + c_2\tau^2 + c_3\tau^3 + c_4\tau^4 + c_5\tau^5 \tag{3.6}$$

and the c_i are calculated such $g(-2) = -2$, $g_\tau(-2) = 0.3$, $g_{\tau\tau}(-2) = 0$, $g(2) = 2$, $g_\tau(2) = 0.3$ and $g_{\tau\tau}(2) = 0$.

In the η-direction the grid is non-uniform and the η points are located at the Chebychev collocation points, see below. Figures 5 and 6 shows the grid lines before and after the mapping for a sample coarse grid. One of the disadvantages of using the standard Chebychev collocation points on the reduced domain $ABCDEF$ is that there is a natural clustering of points near the boundary CD. For the large-gap-width case, this is wasteful of points in regions where they are not needed; a possibly better approach is to use different points in addition to making use of the symmetry as described, for example, in Fornberg (1998 § 5.1).

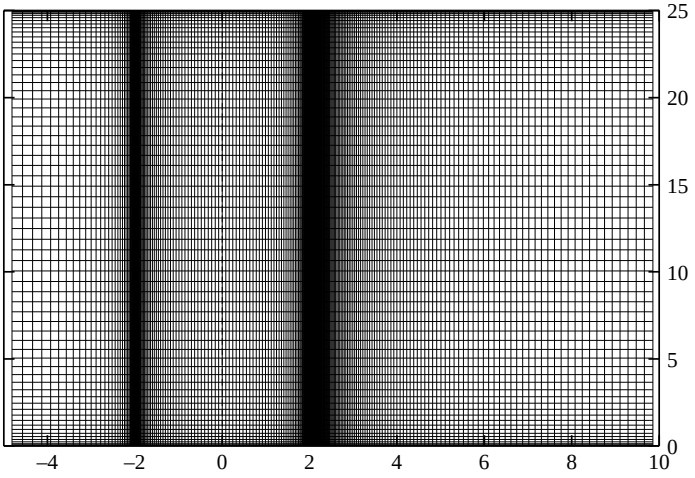

FIGURE 6. Grid lines in the Z-plane.

4. Numerical method

If $\xi = \xi(\tau)$, by using a uniform grid in τ we have to find $|\mathrm{d}Z/\mathrm{d}X|^2$ numerically at each grid point $X_{jk} = x_j + \mathrm{i}y_k$. The equations (3.1) and (3.2) transform to

$$\omega + J(A(\tau)\psi_\tau + B(\tau)\psi_{\tau\tau} + \psi_{\eta\eta}) = 0, \tag{4.1}$$

where J is the Jacobian of the conformal mapping, and

$$A(\tau)\omega_\tau + B(\tau)\omega_{\tau\tau} + \omega_{\eta\eta} + E(\tau)\frac{R}{2}(\psi_\tau\omega_\eta - \psi_\eta\omega_\tau) = 0, \tag{4.2}$$

where $A(\tau) = \partial^2\tau/\partial\xi^2$, $B(\tau) = (\partial\tau/\partial\xi)^2$ and $E(\tau) = \partial\tau/\partial\xi$.

In the τ-direction the domain is truncated to $\tau_{\min} \leqslant \tau \leqslant \tau_{\max}$. A uniform grid in τ is taken with

$$\tau_i = \tau_{\min} + (i-1)h, \qquad i = 1, \ldots m, \tag{4.3}$$

and

$$h = \frac{\tau_{\max} - \tau_{\min}}{m-1}. \tag{4.4}$$

We used fourth-order finite difference in the τ-direction and Chebychev collocation in the η-direction. Thus first and second derivatives in τ are discretized via the difference formulae

$$(\psi_\tau)_{p,j} = \frac{1}{12h}(\psi_{p-2,j} - 8\psi_{p-1,j} + 8\psi_{p+1,j} - \psi_{p+2,j}), \tag{4.5}$$

$$(\psi_{\tau\tau})_{p,j} = \frac{1}{12h^2}(-\psi_{p-2,j} + 16\psi_{p-1,j} - 30\psi_{p,j} + 16\psi_{p+1,j} - \psi_{p+2,j}), \tag{4.6}$$

where $(\psi)_{pj}$ refer to values of the streamfunction at the points τ_p and z_j. Here z_j are the collocation points $\cos(j\pi/n)$, $j = 0, \ldots, n$. The domain $0 \leqslant \eta \leqslant V/2$ is linearly mapped to $-1 \leqslant z \leqslant 1$ and $\eta = \eta_j = (V/4)(z_j + 1)$, $j = 0, \ldots, n$. Then the first derivative in η is given by -

$$\left(\frac{\partial\psi}{\partial\eta}\right)_{p,j} = \sum_{k=0}^{n} D_{j,k}\psi_{p,k},$$

where $D_{j,k}$ are the elements of the Chebychev collocation differentiation matrix $\boldsymbol{D}$, see Caunto, Hussaini & Zang (1987). Similar expressions can be written for the second-derivative terms.

The discretization leads to a set of nonlinear difference equations. Newton–Raphson linearization was used to solve this nonlinear system with $\omega_{ij} = \Omega_{ij} + \overline{\omega}_{ij}$, $\psi_{ij} = \Psi_{ij} + \overline{\psi}_{ij}$ such that $|\Omega_{ij}|, |\Psi_{ij}| \ll 1$ and working with the correction terms Ψ and Ω and where the overbar denotes some initial guess. The linearization together with the discretization leads to a linear system of the form

$$\boldsymbol{A}^{(p)}\boldsymbol{\Phi}_{p-2} + \boldsymbol{B}^{(p)}\boldsymbol{\Phi}_{p-1} + \boldsymbol{C}^{(p)}\boldsymbol{\Phi}_{p} + \boldsymbol{D}^{(p)}\boldsymbol{\Phi}_{p+1} + \boldsymbol{E}^{(p)}\boldsymbol{\Phi}_{p+2} = \boldsymbol{F}^{(p)}, \quad 1 \leqslant p \leqslant m, \tag{4.7}$$

where $\boldsymbol{\Phi}_p = (\boldsymbol{\Psi}_p, \boldsymbol{\Omega}_p)^T$ is the vector of unknown streamfunction and vorticity corrections at each station $\tau = \tau_p$, and

$$\boldsymbol{\Psi}_p = \begin{pmatrix} \Psi_{p0} \\ \vdots \\ \Psi_{pm} \end{pmatrix}, \quad \boldsymbol{\Omega}_p = \begin{pmatrix} \Omega_{p0} \\ \vdots \\ \Omega_{pm} \end{pmatrix}$$

with Ψ_{pj}, denoting the value of the streamfunction at the points $\tau = \tau_p$, $\eta = \eta_j$. Each of the coefficient matrices in (4.7) is a dense matrix arising from the system (2.1) enforced at the collocation points. The matrices $\boldsymbol{A}^{(p)}, \boldsymbol{B}^{(p)}, \boldsymbol{C}^{(p)}, \boldsymbol{D}^{(p)}, \boldsymbol{E}^{(p)}$ are dense matrices of size $2(N+1)$ by $2(N+1)$. The use of fourth-order differences in τ gives rise to the block pentadiagonal structure in (4.7). The linear system was solved for all the vectors $\boldsymbol{\Phi}_p$, $1 \leqslant p \leqslant m$, by using a direct solver, exploiting the sparsity pattern of the block pentadiagonal matrix. The number of unknowns is $2(N+1)m$. Typical values of N and m used in the fine grids are $N = 80, m = 800$.

5. Alternative boundary conditions

One of the difficulties in using a spectral collocation method with the vorticity streamfunction formulation of the Navier–Stokes equations is in the implementation of the no-slip boundary conditions on the body. In the usual finite-difference approximation to these equations some derived local conditions are used for the vorticity on the body surface. In the spectral collocation approach this is inadequate and leads to a degenerate system of equations, see Ehrenstein & Peyret (1989). A different technique has to be adopted and here we use an approach pioneered by Davies & Carpenter (1997) in which some integral constraints are used instead. These integral relations can be derived from Navier–Stokes equations by integration.

At inflow we use the prescribed inflow condition, whereas at outflow we use the conditions

$$\frac{\partial^2 \psi}{\partial \tau^2} = 0,$$

and

$$J\frac{\partial^2 \psi}{\partial \eta^2} + \omega = 0,$$

with $\partial\psi/\partial\tau = 0$ to eliminate the points outside the domain. On $\eta = 0, V/2$ the conditions on Ψ and ω are used.

The no-slip conditions on the cylinder surface cause most difficulty since the conditions $\psi = 0$ and $\partial\psi/\partial\eta = 0$ cannot be imposed directly as this leads to a degenerate

system of equations. The difficulty stems from lack of proper conditions for ω on the cylinder surface.

Using the definition of ω in terms of Ψ

$$J\frac{\partial^2\psi}{\partial\eta^2}+\omega=0,$$

on $\eta=0$ is not enough as this on its own does not guarantee that $\psi_\eta=0$ on $\eta=0$ is satisfied. The boundary conditions $\psi=0, \psi_\eta=0$ imply certain certain integral constraints on the vorticity which need to be satisfied.

In place of the no-slip condition on the tangential velocity component, we instead use the following integral constraint. From

$$\left\{\frac{\partial^2\psi}{\partial\xi^2}+\frac{\partial^2\psi}{\partial\eta^2}\right\}J+\omega=0,$$

we obtain

$$\int_{\eta=0}^{V/2}\left(\frac{\partial^2\psi}{\partial\xi^2}+\frac{\omega}{J}\right)\mathrm{d}\eta+\left[\frac{\partial\psi}{\partial\eta}\right]_{\eta=0}^{V/2}=0. \tag{5.1}$$

This was used together with $\psi=0$ in place of the no-slip condition at $\eta=0$. A test on the accuracy of the method is how well the no-slip condition is satisfied on $\eta=0$. It was found that this was satisfied to the same tolerance as the rest of the discrete equations. For additional points concerning the numerical method see Azzam (2003).

6. Results and discussion

Results for the flow past a cascade of circular cylinder were obtained for various values of Reynolds numbers and various gap widths. Extensive checks were made to validate the code and to check for grid independence and sensitivity to domain truncation both upstream and downstream. Typically calculations were carried out with 81 Chebychev nodes and between 600 and 800 points in the ξ-direction. It was found that the calculations were most sensitive to the location of the upstream boundary for large gap widths. For most of the calculations $\tau_{\min}=-7$ (with a corresponding $x_{\min}$ value between -100 and -90) was used and decreasing $\tau_{\min}$ did not cause any significant change in the results. The value of $\tau_{\max}$ was set to a large enough value to ensure that the eddy was contained in the computational domain. Setting $\tau_{\max}$ to be smaller than the eddy length resulted in only part of the eddy being computed. The boundary conditions used at the downstream end allowed the eddy to pass smoothly out of the domain.

In the η-direction the standard collocation points $\eta_j=\cos(j\pi/M)$ were used. Except for a few points in R-space, and in particular for large W, the convergence pattern was quadratic and the solution was obtained in a few Newton iterations. The solution at a previous value of the Reynolds number was used as a starting value in most of the computations. Difficulty in convergence was experienced for $W=100$, near $R=400$ where continuation to the next value in R-space required very small increments in R. The reason for the difficulties in convergence at some of these points in parameter space may be attributed to a change in solution properties near critical values, as can be seen for example in the change in the sensitivity to grid size changes near these values.

$W \backslash R$		100	200	400	600	800
5	F	10.0	18.6	35.5	52.3	69.1
5	P	10.0	18.6	35.5	52.2	68.9
20	F	11.9	22.0	41.5	60.6	79.3
20	P	11.9	22.0	41.7	61.1	80.2
100	F	13.2	26.1	56.1	84.5	105
100	P	13.3	26.2	56.6	88.6	114

TABLE 2. Comparison of the length of recirculation region between the present results (P) and Fornberg's (1991)(F).

6.1. *Grid dependence studies*

Extensive grid dependence tests were made to check that the results obtained on the finest grids were grid independent. The behaviour of various flow properties such as the length of the eddy, its width, maximum vorticity on the body surface and drag coefficients, was compared for a varying number of point in the τ-direction and a varying number of Chebychev collocation points. Figures showing the results of these comparisons and other grid-dependence studies are available as a supplement to the online version of this paper or from the authors or JFM Editorial office, Cambridge. They show that the $W = 5$ results are fully resolved up to $R = 4000$. Results for the $W = 20$ case show that they are fully resolved on the finest grids used for these gap widths. For a gap width of $W = 5$ even a coarse grid with as few as 32 Chebychev points in the vertical direction is enough to obtain reasonable results.

The same is not true however for increasing gap widths. The length of the eddy appears to be the most sensitive quantity to compute accurately. For $W = 50$, the length of the eddy is sensitive to the number of points used, and the accuracy also depends on the Reynolds number. At least 64 points and at least $h = 1/20$ are necessary for low Reynolds numbers for this case. For higher Reynolds numbers ($R > 800$) the number of Chebychev points required to resolve the flow features increases. At the larger Reynolds numbers, the results for eddy length on the finest grid ($N = 100, h = 1/30$) suggest converged values especially for the eddy width, and drag.

The $W = 100$ gap width case is even harder to compute accurately for the high Reynolds numbers. The only computed quantity which is grid independent is the eddy width. The length of the eddy can be accurately computed up to about $R = 700$. At a Reynolds number of 800 there is about 10% difference in the results between the three finest grids used. At larger Reynolds numbers the differences are much larger.

One may conclude therefore that whereas for small gap widths the flow feature can be resolved using fairly coarse grids, for larger gap widths, using a coarse mesh can cause huge differences in the overall solution properties, particularly for the length of the eddy. It was not possible to compute with even finer meshes because of computer resource limitations.

6.2. *Comparison with Fornberg* (1991)

A comparison of our results with those of Fornberg (1991) is given in tables 2–5 for the eddy length and width for selected values of W and R. It is seen that our results agree well with those of Fornberg (1991) for the small gap widths. For the

$W\backslash R$		100	200	400	600	800
5	F	1.97	2.09	2.17	2.20	2.22
5	P	1.70	2.093	2.167	2.1997	2.217
20	F	2.71	3.37	3.98	4.26	4.75
20	P	2.69	3.35	3.96	4.24	4.75
100	F	2.88	3.98	9.02	24.1	35.1
100	P	2.864	3.993	9.390	25.93	37.32

TABLE 3. Comparison of the width of recirculation region between the present results (P) and Fornberg's (1991)(F).

$W\backslash R$		100	200	400	600	800
5	F	17.8	25.1	35.4	43.4	50.0
5	P	17.87	25.18	35.67	43.78	50.64
20	F	10.3	14.5	20.6	25.3	29.3
20	P	10.28	14.54	20.76	25.62	29.72
100	F	9.2	12.6	16.7	17.6	18.6
100	P	9.157	12.56	16.64	17.31	18.54

TABLE 4. Comparison of the maximum vorticity on body surface the between present results (P) and Fornberg's (1991) (F).

$W\backslash R$		100	200	400	600	800
5	F	2.974	2.543	2.278	2.47	2.10
5	P	2.988	2.563	2.313	2.218	2.168
20	F	1.248	1.028	0.906	0.86	0.831
20	P	1.256	1.039	0.9229	0.883	0.8618
100	F	1.072	0.847	0.672	0.50	0.424
100	P	1.08	0.8485	0.6581	0.4897	0.4245

TABLE 5. Comparison of the drag coefficient between the present results (P) and Fornberg's (1991) (F).

larger gap widths, in particular $W = 100$, the agreement is good up to $R = 400$, but for Reynolds beyond this value, there are some differences, particularly in the length of the eddy. For $W = 100$ and $R = 800$ the difference between the two results is about 10%. The difference in the width of the eddy at the same value of the Reynolds number is smaller. There may be several reasons for the discrepancies. In Fornberg (1991) the large-W results were obtained with a modified version of the code. In our case the same code has been used for all gap widths. In addition in Fornberg (1991) the results were computed with a second-order method in both directions whereas the method used here is of fourth order in one direction and spectral in the other direction. Thus overall our method has greater accuracy. On the other hand the grid dependence studies do not indicate converged values for the eddy length at $R = 800$.

6.3. *Streamline and vorticity plots for different gap widths*

Our numerical results indicate that at least three distinct types of solution exist, depending on the gap width. The first type (I) is shown in figures 7 and 8 where the streamline and vorticity contours are plotted for $W = 5$ for various values of

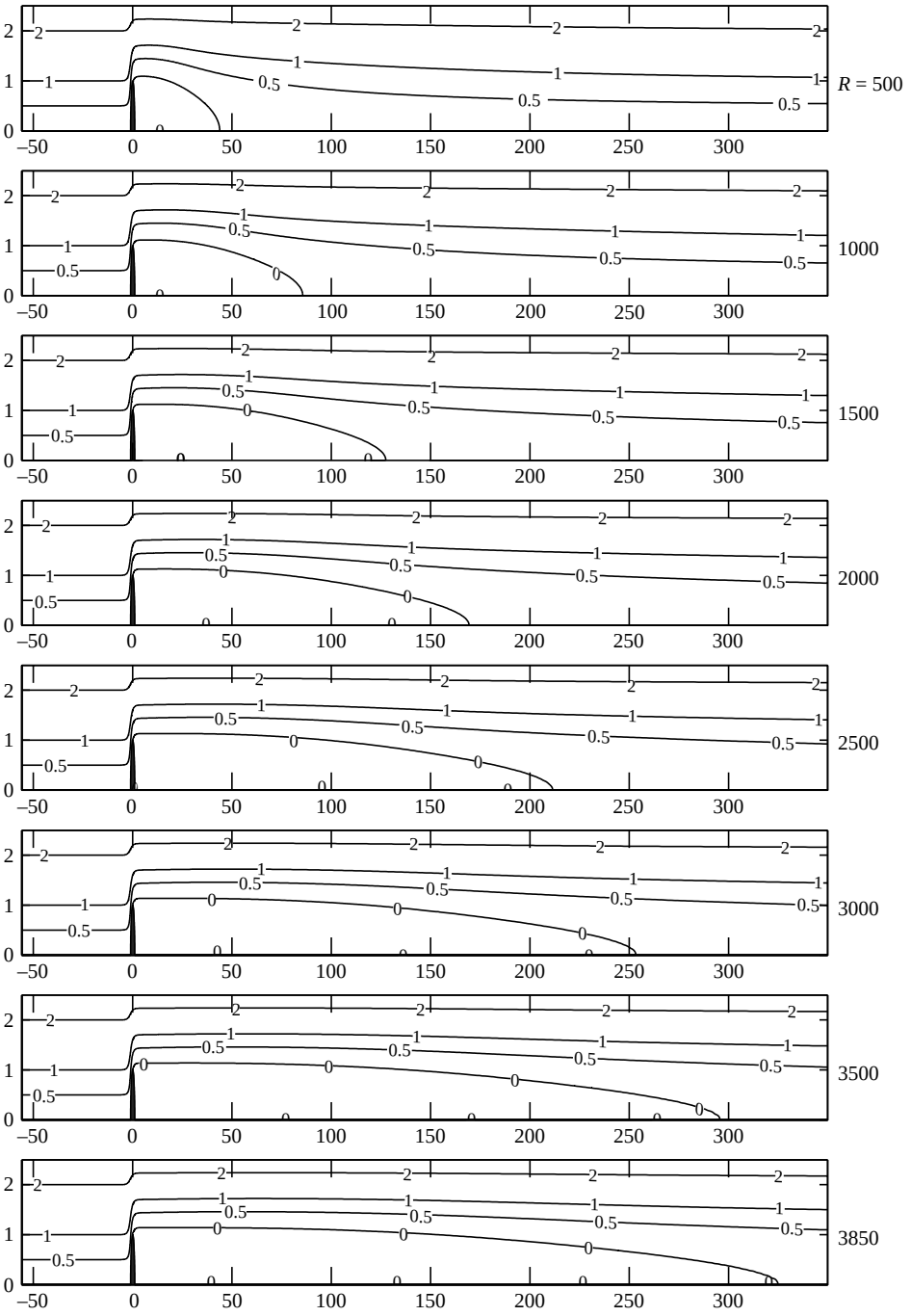

FIGURE 7. Streamfunction contours for $W = 5$.

the Reynolds number. The type I solutions show the presence of a long thin eddy behind the cylinder with the eddy length increasing with Reynolds numbers. It is noticeable in figure 8 that the vorticity in the eddy region is not constant. The eddy length is plotted as a function of Reynolds number in figure 9 and the length is

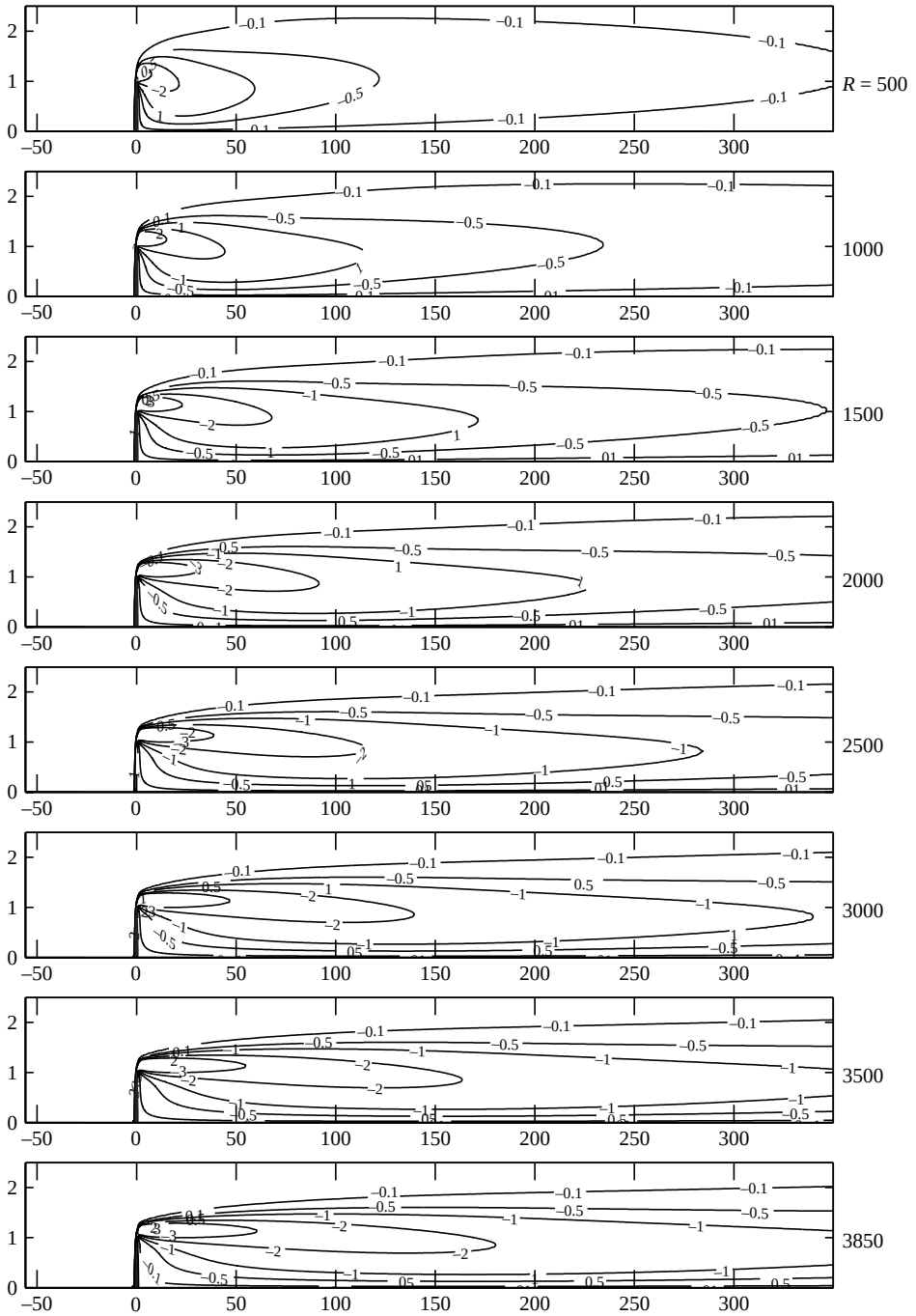

FIGURE 8. Vorticity contours for $W = 5$. The contour levels plotted are $-3,-2,-1,-0.5,-0.1,1,2,3,4,6$.

found to increase linearly with the Reynolds number. In figure 9 the eddy width is plotted against R and this shows the width remaining constant with increasing R. The values of the various flow quantities such as eddy length L, eddy width Wi, maximum

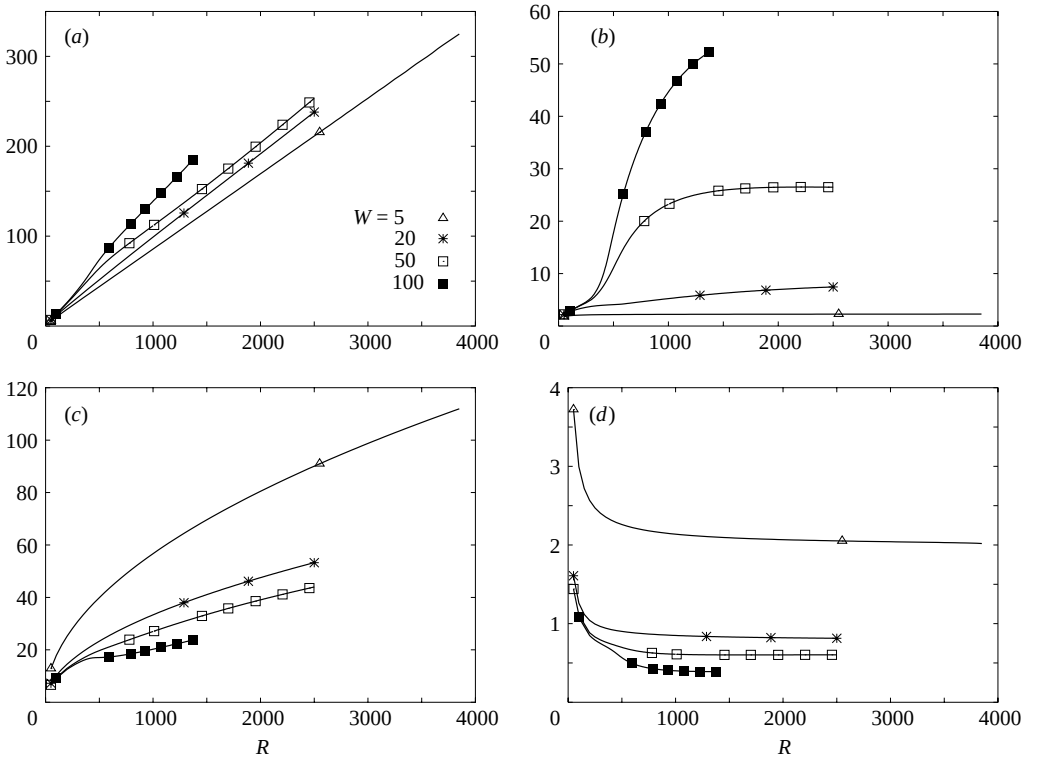

FIGURE 9. Various flow quantities for $W = 5, 20, 50$ and 100 against Reynolds number taken from the finest grid: (*a*) eddy length, (*b*) eddy width, (*c*) maximum vorticity on body surface, and (*d*) drag.

R	L	Wi	ω_{max}	D
100	10.03	1.970	17.87	2.994
500	43.85	2.186	39.92	2.260
1000	85.64	2.228	56.69	2.137
1500	127.5	2.246	69.59	2.092
2000	169.4	2.257	80.48	2.068
2500	211.4	2.265	90.07	2.052
3000	253.4	2.271	98.74	2.041
3500	295.7	2.276	106.7	2.031

TABLE 6. The length of the eddy L, its width Wi, maximum vorticity on the surface of the cylinder ω_{max}, and the drag coefficient D for $W = 5$.

vorticity on the cylinder ω_m and drag D are tabulated in table 6 for some selected Reynolds numbers.

The drag coefficient D can be evaluated as a line integral along the cylinder surfaces corresponding to the relation (in polar coordinates):

$$D = \frac{4}{R}\int_0^{\pi}\left(\frac{\partial\omega}{\partial r} - \omega\right)\sin(\theta)\,\mathrm{d}\theta. \tag{6.1}$$

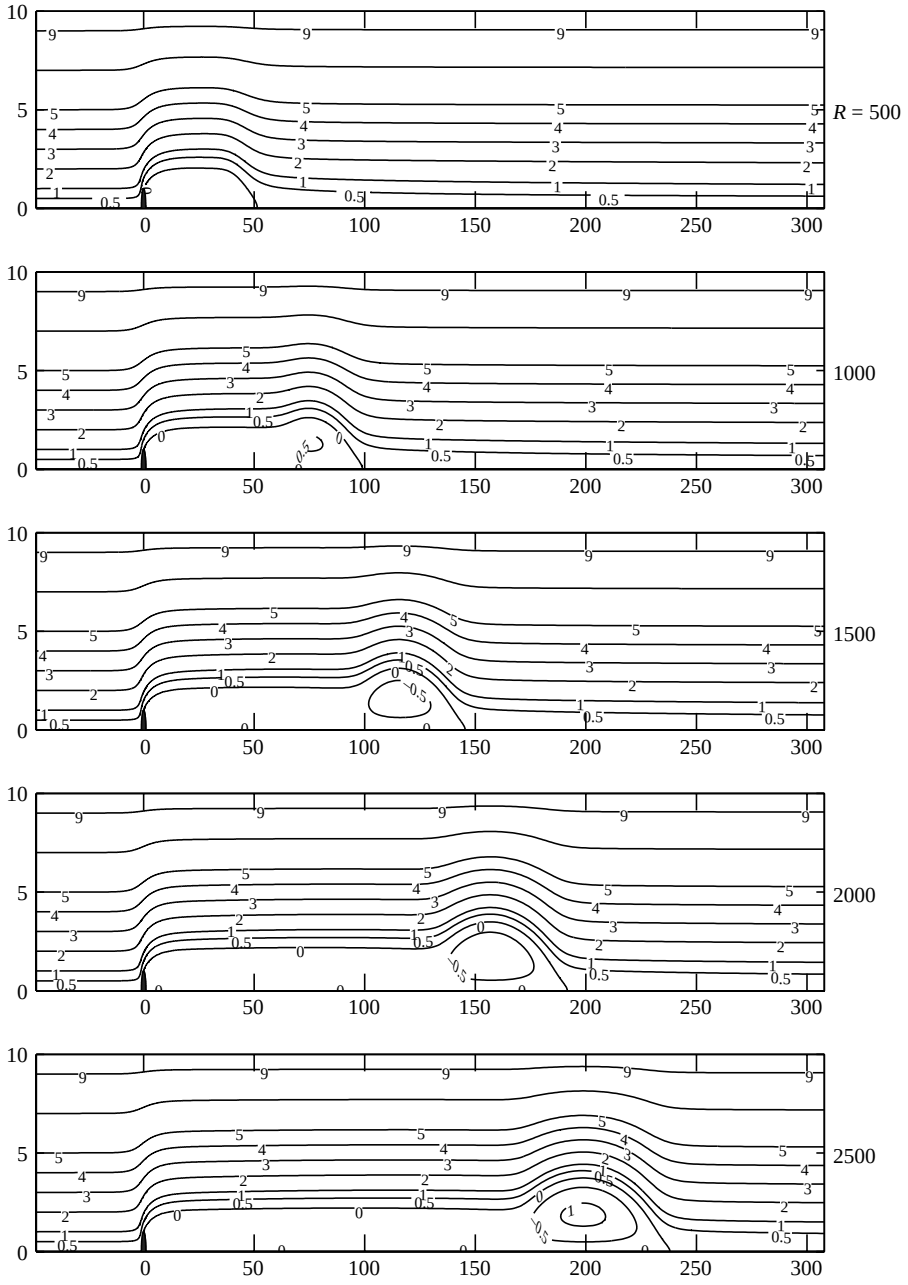

FIGURE 10. Streamfunction contours for $W = 20$. The contour levels plotted are 9,7,5,4,3,2,1,0.5,0,−0.5,−1.

The solution features found here for small gap widths are not dissimilar to the boundary layer type solutions for the wake discussed by Smith (1985*a*) and Milos & Acrivos (1986).

As the gap width increases, the solution properties alter considerably from those for narrow gaps, giving rise to a type II solution. This can be seen clearly in the streamline and vorticity contours for $W = 20$ shown in figures 10 and figure 11. Behind

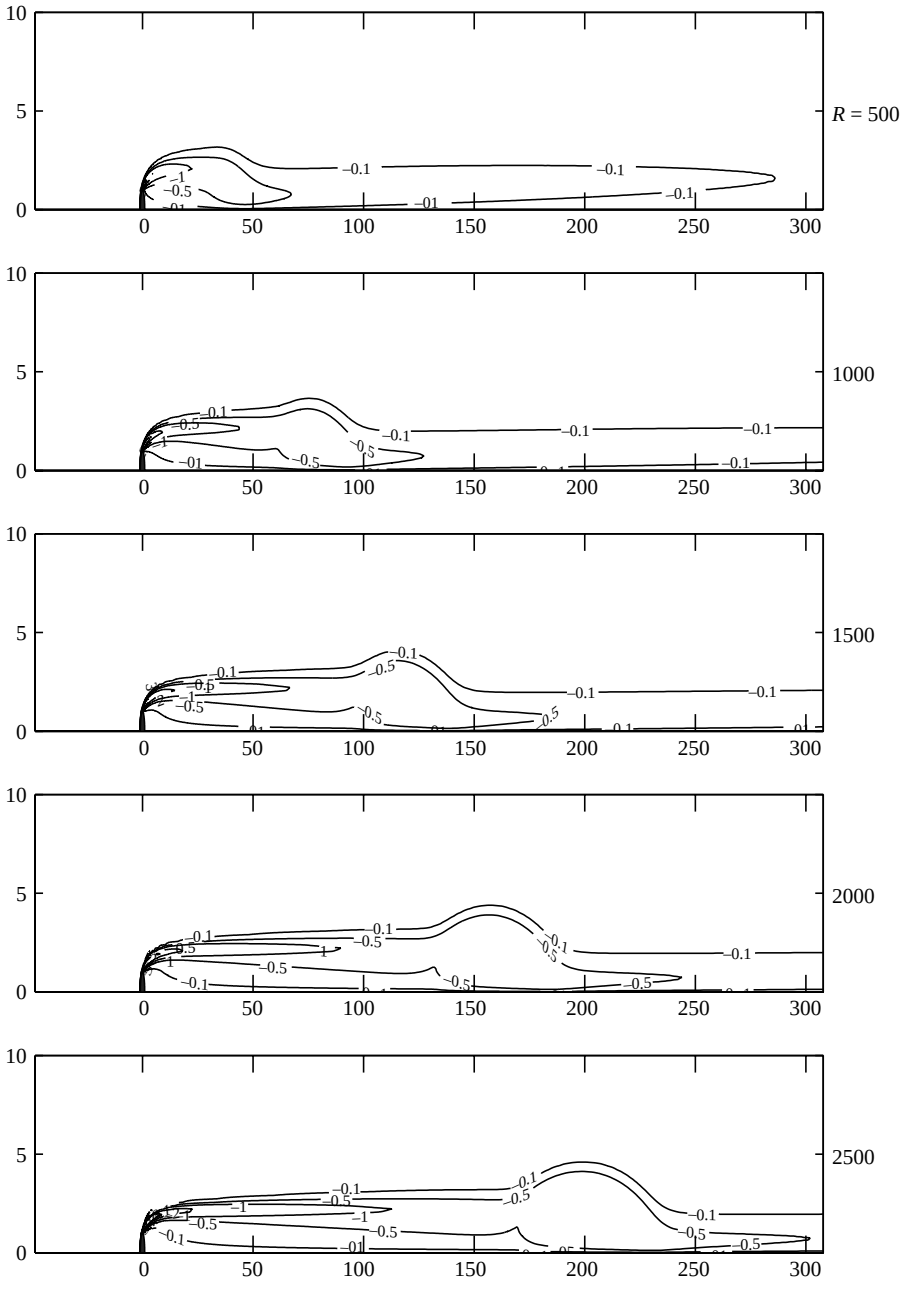

FIGURE 11. Vorticity contours for $W = 20$. The contour levels plotted are $-3,-2,-1,-0.5,-0.1,1,2,3,4,6$.

the cylinder there is a long thin eddy, but near reattachment, the eddy width increases abruptly. The eddy structure for a type II solution is a combination of a long thin eddy with a Sadovskii (1971) type of vortex near reattachment. The eddy length and width as a function of Reynolds number were shown in figure 9. The length is seen to increase linearly with increasing Reynolds number. The eddy width increases

R	L	Wi	ω_{max}	D
100	11.92	2.692	10.28	1.260
500	51.43	4.083	23.30	0.9009
1000	98.97	5.231	33.35	0.8496
1500	145.4	6.257	41.06	0.8305
2000	191.6	6.978	47.55	0.8202
2500	238.0	7.455	53.26	0.8138

TABLE 7. The length and width of the eddy, maximum vorticity and drag coefficient for $W = 20$.

R	L	Wi	ω_{max}	D
100	13.10	2.858	9.371	1.110
500	64.27	11.10	19.71	0.6982
1000	111.6	23.22	27.00	0.6106
1500	156.5	25.91	33.47	0.6023
2000	203.9	26.47	39.06	0.6026
2500	253.3	26.48	43.97	0.6037

TABLE 8. The length of the eddy, width, max. vorticity and the drag coefficient for $W = 50$ taken from the finest grid with $N = 100$, $h = 1/30$.

R	L	Wi	ω_{max}	D
100	13.28	2.865	9.157	1.079
500	73.74	17.75	17.06	0.5676
700	101.9	32.30	17.84	0.4498
900	126.7	41.37	19.36	0.4092
1200	163.3	49.48	22.10	0.3916
1400	188.5	52.64	24.00	0.3899

TABLE 9. The length of the eddy, width, max. vorticity and the drag coefficient for $W = 100$ taken from the finest grid with $N = 111$, $h = 1/30$.

with Reynolds number but levels out for large Reynolds numbers. Selected numerical values are tabulated in table 7.

For large gap widths, the solution properties for the isolated cylinder case are expected to emerge and this can be seen clearly in the results for $W = 50$ shown in figures 12 and 13 and for $W = 100$ shown in figures 14 and 15. Selected numerical values are tabulated in tables 8 and 9 respectively. This is another distinct type of solution found which we label type III. Here the presence of a large Sadovskii vortex behind the cylinder is seen with the dimensions increasing with Reynolds numbers. The cylinder appears as a point on the scale of the eddy. The vorticity contours clearly show the region of uniform vorticity inside the eddy. The trend for the eddy length is increasing linearly as before, but the eddy width for fixed gaps cannot increase indefinitely, and changes behaviour as the Reynolds numbers increases beyond a critical value as seen in figure 9, see also table 9.

In figure 16 we show perspective plots of the vorticity and streamwise velocity for the three different types of solutions at selected Reynolds numbers for gap widths of $W = 5, 20$ and 50. For the larger gap widths these show clearly the flat region of constant vorticity inside the eddy.

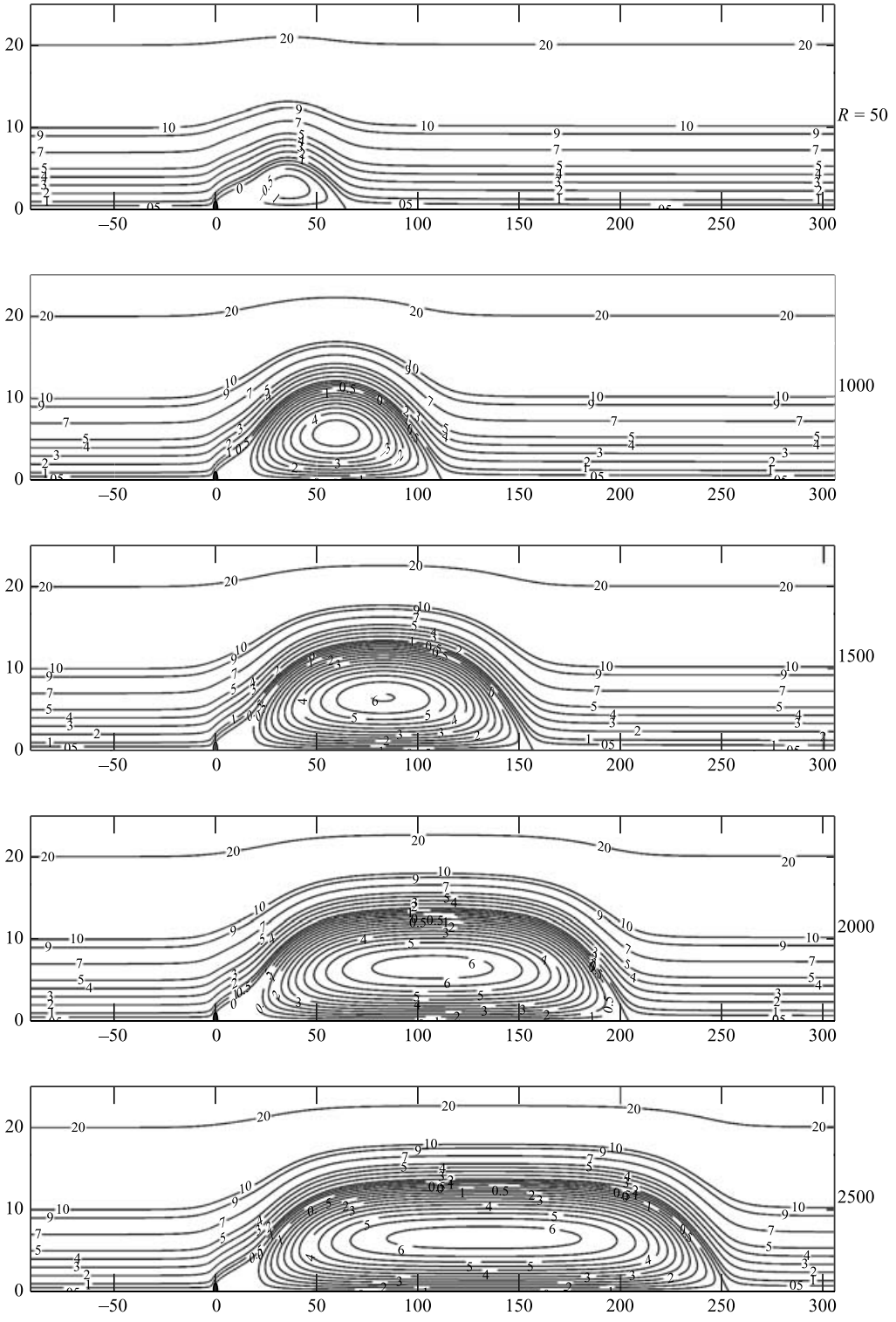

FIGURE 12. Streamfunction contours for $W = 50$. The contour levels plotted are 20,10,9,7,5,4,3,2,1,0.5,0,−0.5,−1,−1.5,−2,−2.5,−3,−3.5,−4,−4.5,−5,−5.5.

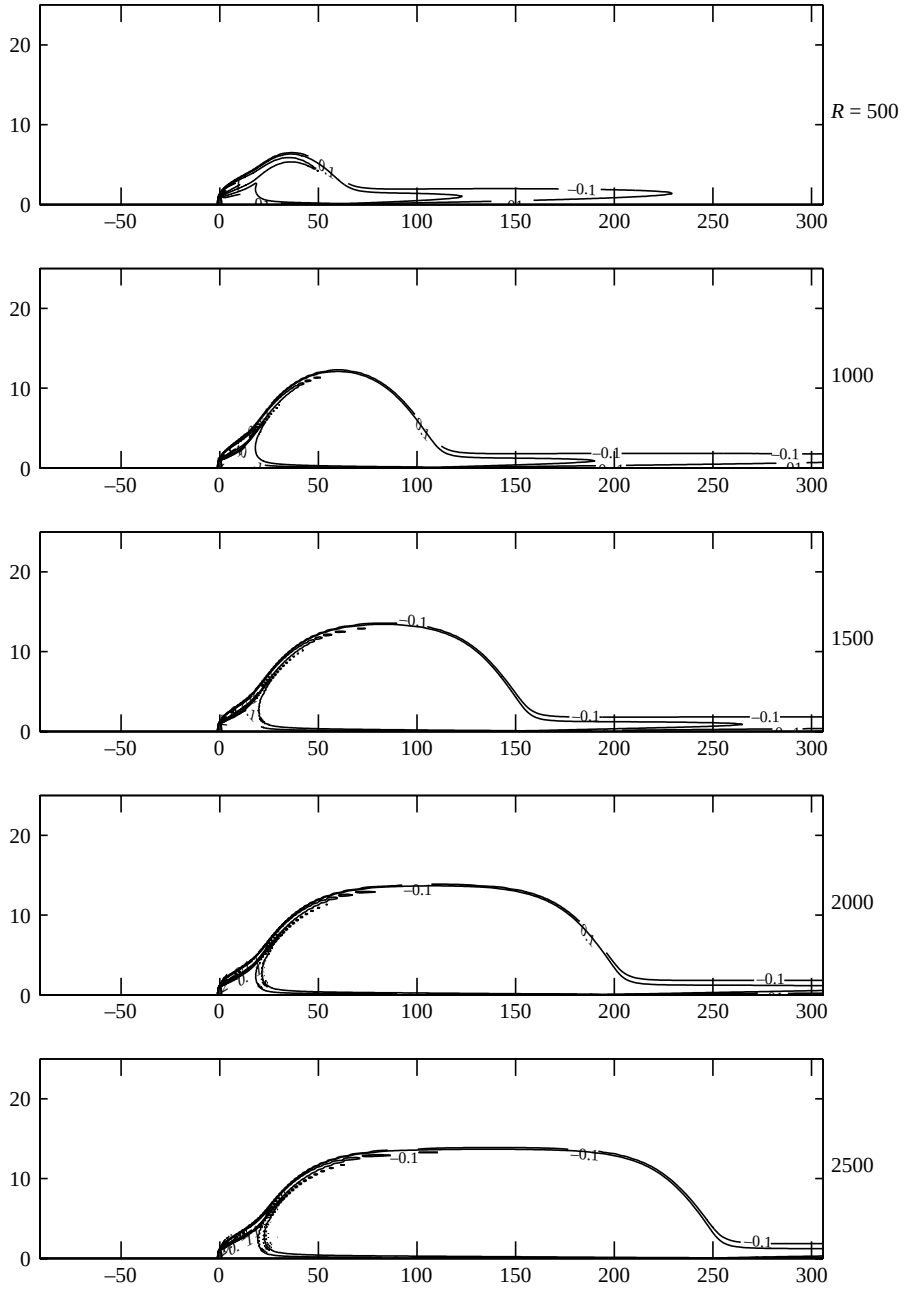

FIGURE 13. Vorticity contours for $W = 50$. The contour levels plotted are $-3,-2,-1,-0.5,-0.2,-0.1,1,2,3,4,6$.

6.4. *Comparison with theoretical predictions*

Theoretical results for the steady flow past an isolated (single) bluff body and a cascade of bluff bodies are described in the review article by Chernyshenko (1998). The theory for the isolated bluff body is more developed than that for a row of bluff bodies, but nevertheless some predictions are available for the behaviour of certain

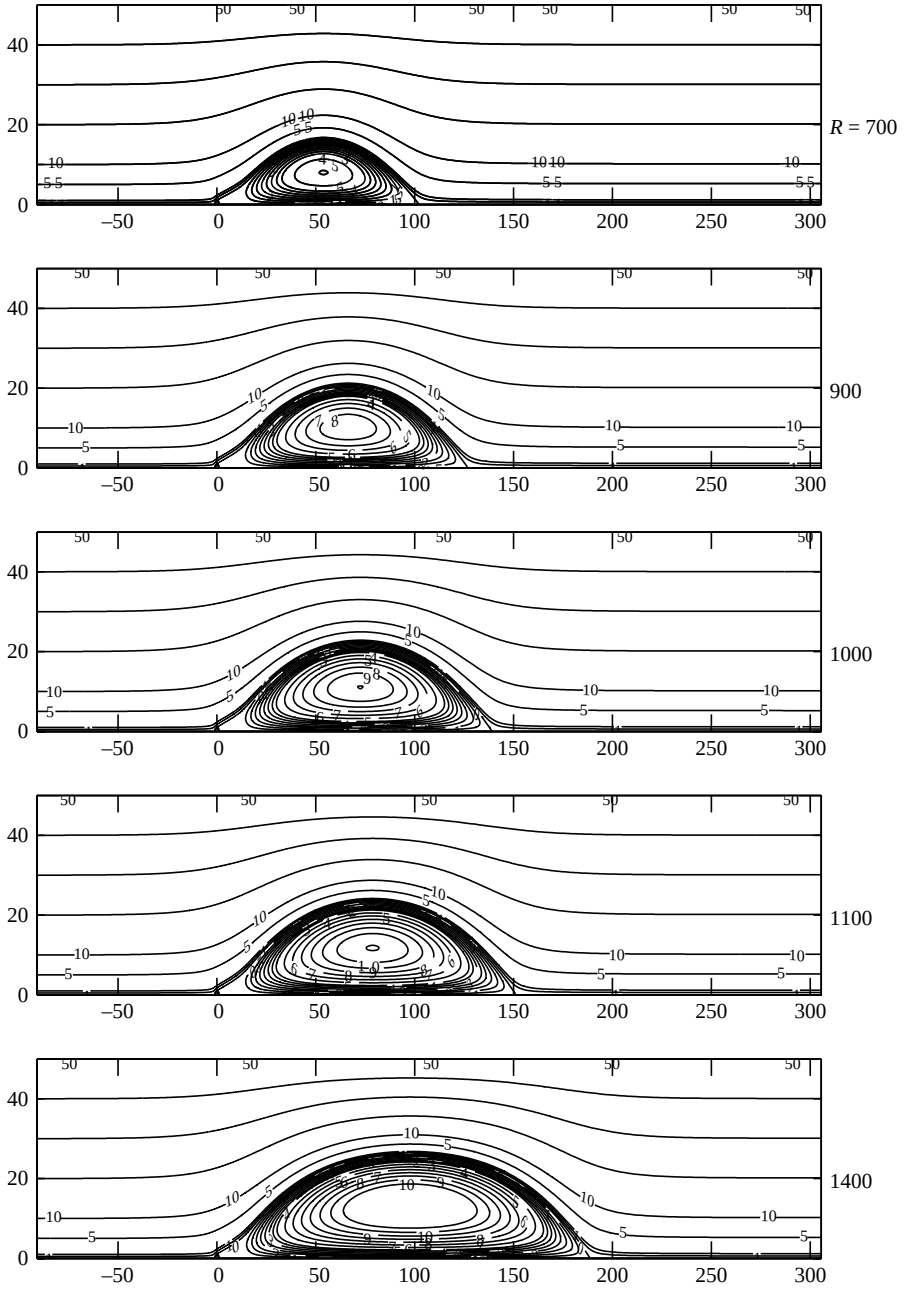

FIGURE 14. Streamfunction contours for $W = 100$. The contour levels plotted are 50,40,30,20,10,5,1,0.5,0,−0.5,−1,−1.5,−2,−2.5,−3,−3.5,−4,−5,−6,−7.

global properties. The principal results, see Chernyshenko & Castro (1993), may be described as follows. Let L be the length of the eddy and Wi be the eddy width. We also let $Re = R/2$ be the Reynolds number based on radius. Then under certain conditions, which are discussed more fully in Chernyshenko & Castro (1993), the

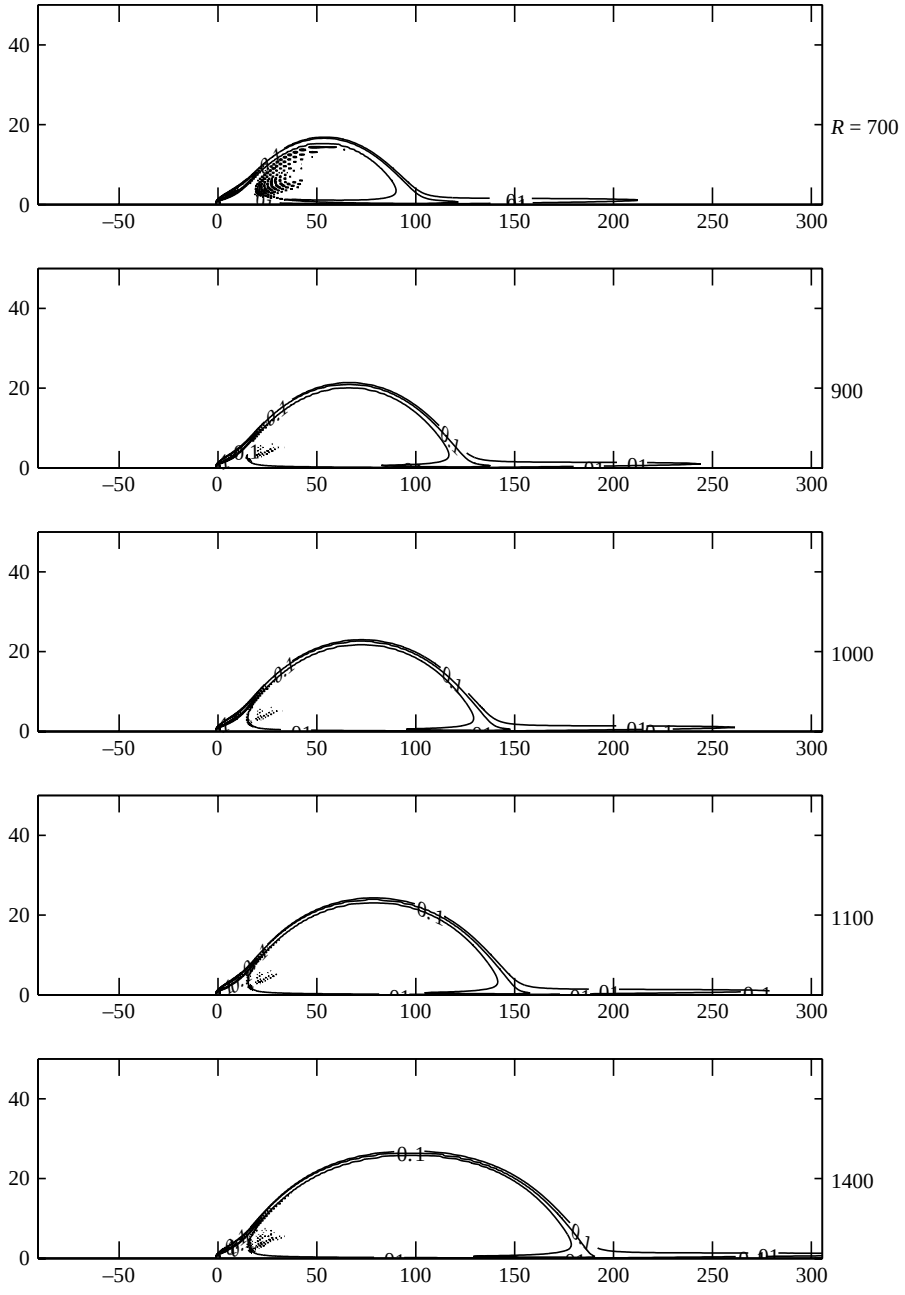

FIGURE 15. Vorticity contours for $W = 100$. The contour levels plotted are $-3,-2,-1,-0.5,-0.2,-0.1,0.1,1,2,3,4,6$.

following estimates hold:

$$\omega_d k_d^2 Re = 2C D_0^2(b), \tag{6.2a}$$

$$L/\left(k_d^2 Re\right) = 1/\left[2D_0^2(b)(\alpha C)^{1/2}\right], \tag{6.2b}$$

$$Wi/\left(k_d^2 Re\right) = W/\left[2L D_0^2(b)(\alpha C)^{1/2}\right]. \tag{6.2c}$$

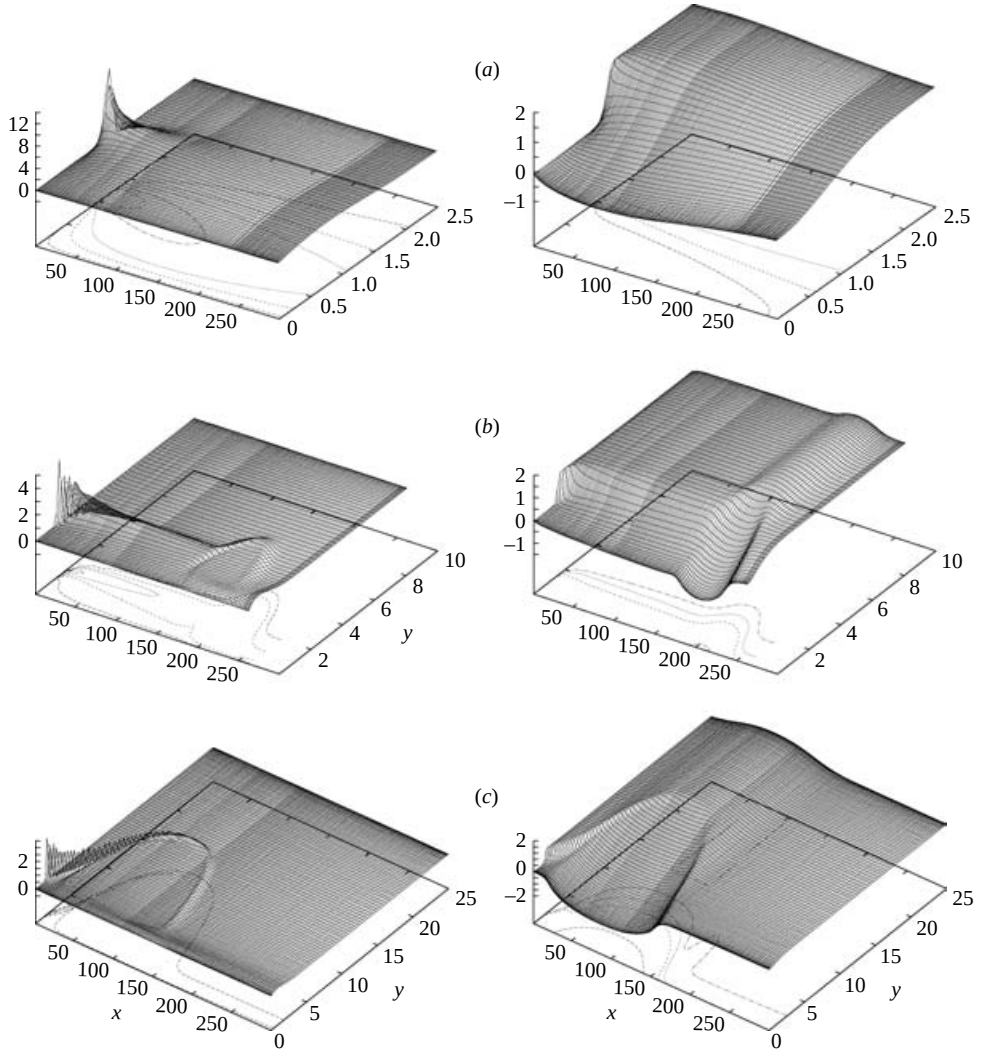

FIGURE 16. Perspective plots of the vorticity (left) and streamwise velocity (right) for (*a*) $R = 3000$, $W = 5$, (*b*) $R = 2500$, $W = 20$, and (*c*) $R = 1500$, $W = 50$.

Here the right-hand sides of (6.2) contain various quantities such as $C, D_0(b), \alpha$ which are all functions of W/L and arise in the asymptotic theory. The values of these functions are tabulated in Chernyshenko (1993). Also, ω_d is the value of the (constant) eddy vorticity inside the Sadovskii vortex, and k_d is a constant stemming from the condition of smooth separation past a bluff body. For an isolated circular cylinder $k_d = 1/2$ but the value $k_d = 0.45$ has been used when making comparisons by Chernyshenko & Castro (1993) on the grounds that there is a weak dependence of k_d on Re. There are additional assumptions regarding the validity of the theory as described in detail by Chernyshenko & Castro (1993). For the case $(W/L) \to 0$, $W \gg 1$ the predictions reduce to

$$\omega_d \to \frac{9}{W}, \tag{6.3a}$$

$$c_d Re \to 91.3 k_d^2 Re/W, \tag{6.3b}$$

$$Wi/L \to 2W/\left(2.538 k_d^2 Re\right). \tag{6.3c}$$

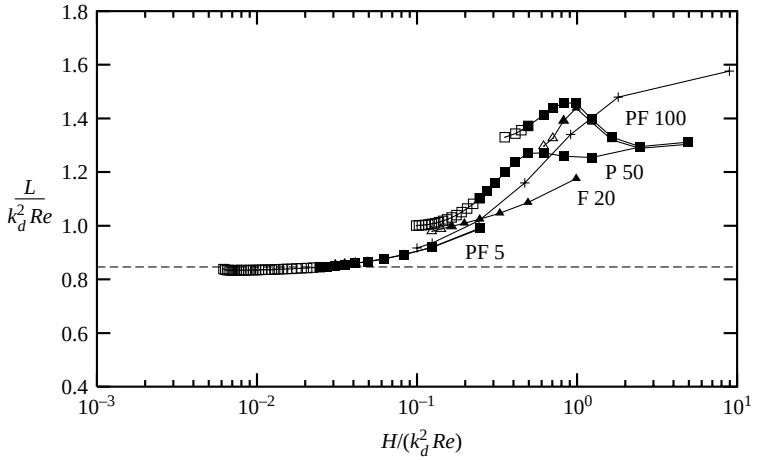

FIGURE 17. Eddy length as a function of $W/k_d^2 Re$. The triangles show the results of Fornberg (1991) (marked F with the W value also shown) for different Reynolds numbers from $R = 100$ to 800 in intervals of 100. The squares show the present results (marked P) from $R = 100$ to R_m in intervals of R_{int}. For $W = 5$, $R_m = 4000$, $R_{int} = 100$ for $R < 1000$ and $R_{int} = 500$ for $R > 1000$. For $W = 50$, $R_m = 2500$, $R_{int} = 100$. For $W = 100$, $R_m = 1400$, $R_{int} = 100$. Increasing Reynolds numbers are shown going from solid to open symbols. The solid and dashed curves are from the asymptotic predictions (6.2) and (6.3) respectively.

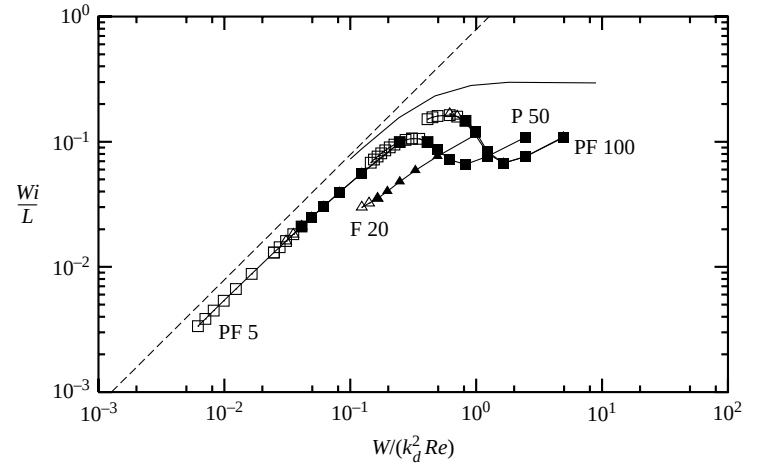

FIGURE 18. The ratio of the eddy half-width to the eddy length as a function of $W/k_d^2 Re$. For symbols and line styles see the caption to figure 17.

Comparison of the eddy length with the prediction (6.2*a*) and (6.3*b*) is shown in figure 17. As in Chernyshenko & Castro (1993) the Reynolds number increasing is shown by going from solid to open symbols, but no additional meaning is attached to when the symbols change from solid to open. The agreement between the theory and numerical results is particularly good for the narrow gap width case. For larger gap widths, the present results show no sign of approaching the theoretical curve, although the results of Fornberg (1991) are better in this respect. In figure 18 the ratio of the eddy half-width to eddy length is compared with (6.2*c*) and (6.3*c*). Again

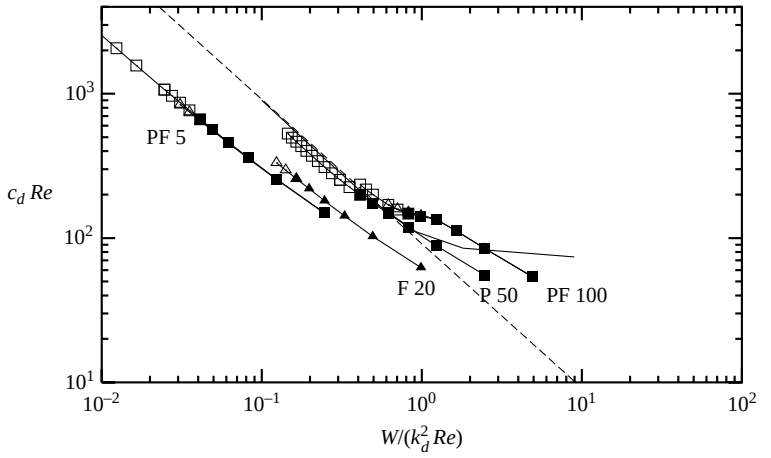

FIGURE 19. $c_d Re$ as a function of $W/k_d^2 Re$. For symbols and line styles see the caption to figure 17.

for $(W/L) \to 0$ the agreement with the predicted asymptote is good. Similar results for the eddy drag shown in figure 19 agree well with the predictions.

One important point to note is that the numerical results for the eddy vorticity approach a constant value only for large gap widths. For W small, the contour plots of the vorticity in figure 8 shows that the vorticity is not constant in the long and slender eddy. The theoretical asymptotes (6.3) are based on the assumption of a Sadovskii vortex with constant eddy vorticity, and thus the good comparison seems somewhat surprising and may be fortuitous. It is possible that some of the global estimates used in deriving the asymptotic predictions apply equally to other models of the flow in wakes in the limit of $(W/L) \to 0$. In the work of Acrivos *et al.* (1965) the flow in the slender eddy is described by the boundary layer equations, and the vorticity is not assumed to be constant, see also Smith (1985*a*), Bhattacharya, Dennis & Smith (2001).

6.5. *Type I boundary layer solutions: comparisons with theory*

Let us now try to assess some of the theoretical implications of the work by Smith (1985*a*) and Milos & Acrivos (1986). In these papers it is suggested that because the eddies are long and thin compared to the lateral dimension y it is appropriate to consider boundary layer scalings with $x = RX$, $y = O(1)$ and take the limit $R \gg 1$. In this case the Navier–Stokes equations reduce to the boundary layer equations, see Smith (1985*a*),

$$U U_X - \psi_X U_y = -P_X + U_{yy}, \quad \psi_y = U, \tag{6.4}$$

with boundary conditions

$$\psi = U_y = 0 \quad \text{on} \quad y = 0, \quad \psi = W/2, U_y = 0 \quad \text{on} \quad y = W/2,$$

for $X > 0$. Also $U \to 1$ as $X \gg 1$. The starting conditions at $X = 0+$ are different in the two papers. In Smith (1985*a*) the conditions

$$X = 0+, \quad U = \begin{cases} 0 & \text{for} \quad 0 < y < \lambda \\ (W/2)/((W/2) - \lambda) & \text{for} \quad \lambda < y < W/2 \end{cases}$$

are used. In Milos & Acrivos (1986) the starting conditions are taken to be

$$U(X=0+, y)=\begin{cases}-u_c(y), & 0\leqslant y\leqslant \lambda/2,\\ u_c(1-y), & \lambda/2\leqslant y<\lambda\\ u_0(y), & \lambda<y<W/2.\end{cases}$$

Here λ is the eddy width, $u_c(y)$ is the (unknown) reverse flow that enters the inviscid region from the boundary layer region, and $u_0(y)$ is the prescribed streamwise velocity above the eddy boundary. For the problem at hand a suitable choice for $u_0(y)$ would be $u_0(y)=(W/2)/((W/2)-\lambda)$. It should also be mentioned that the Milos & Acrivos (1986) paper was concerned with describing the experiments of Acrivos *et al.* (1965) and Acrivos *et al.* (1968) in which a splitter plate was used behind the cylinder and because of this the no-slip condition $U=0$ is imposed on $y=0$ in their subsequent computations of the boundary layer equations. This apart, the principal difference between the Smith (1985*a*) and Milos & Acrivos (1986) suggestions is in the form of the eddy velocity prescribed at inflow. A more detailed description of the matching of the boundary layer flow to that near the cylinder is given in Smith (1985*a*).

Smith (1985*a*) has shown that the equations can be rescaled to involve just one parameter: $H=2\lambda/W$. Some solutions of the boundary layer problem (6.4) are presented in Smith (1985*a*). For small values of H difficulties were encountered in obtaining grid-independent solutions. For $W=5$ we can make some qualitative as well as quantitative comparisons with the results of Smith (1985*a*). From the numerical data for $W=5$, $\lambda=1.13$ approximately, giving a value of $H=0.452$. From the boundary layer problem (6.4) the length of the eddy can be estimated as $L_s=(R/2)(W/2)^2x_{att}$ where x_{att} is the reattachment length given by the normalized problem involving H. The factor of $R/2$ arises because of the Reynolds number based on the diameter, and the other factor stems from the normalization, see Smith (1985*a*, equation *I*2.7). For a value of $H=0.452$ the results of Smith (1985*a*) give $x_{att}=0.023$ approximately, giving $L_s=0.072R$. Our Navier–Stokes computations give $L=0.084R$ for $W=5$ which is in excellent agreement with the theoretical result. For $W=20$, our results suggest that $\lambda=2$ approximately, giving $H=1/5$. For small values of H, Smith (1985*a*) reported difficulties in obtaining converged results and therefore direct comparison with Smith (1985*a*) for $H=0.2$ is not possible.

In figures 20 and 21 we show centreline and edge velocities from the Navier–Stokes computations. These may be compared directly with figure 5 in Smith (1985*a*). The trends for the edge velocity for large H (implying small W in our case) are broadly similar. For H decreasing (W increasing), the Navier–Stokes data shows the presence of a bulge in the edge velocity near reattachment. In the boundary layer solutions of Smith (1985*a*), the initial trend for the edge velocity is similar but no such bulge exists. Of course as remarked already, at these values of H the results of the boundary layer calculations are not grid independent and probably unreliable for large values of X.

In figures 22–24 we plot graphs of the streamfunction and vorticity and velocity as a function of y for various x locations from the Navier–Stokes data for selected Reynolds numbers and different gap widths. It is clear that for $W=5$ as we approach the cylinder, the initial streamwise velocity in the eddy region is small and negative. In Smith (1985*a*) the initial profile used assumes zero velocity in the eddy to leading order. Exactly what difference taking a non-zero eddy velocity makes to the results remains unclear.

For the type II solutions, figure 23 shows that downstream just prior to the formation of the eddy, the streamwise velocity decreases significantly. The velocity in

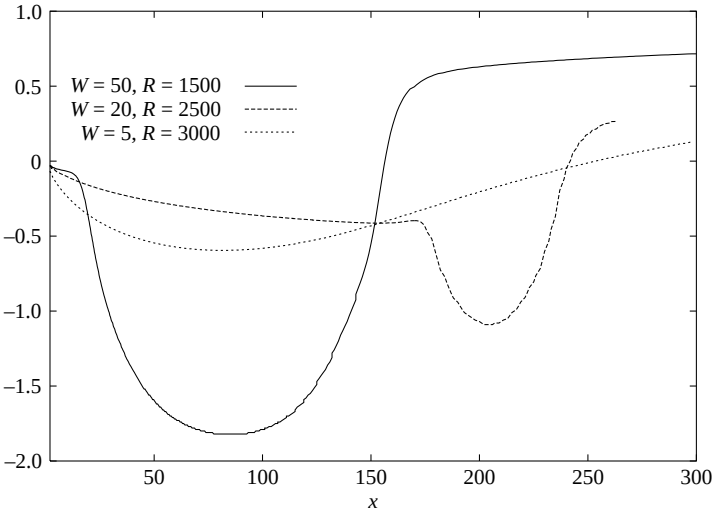

FIGURE 20. Centreline velocity from the Navier–Stokes computaions for $R = 3000$, $W = 5$; $R = 2500$, $W = 20$; $R = 1500$, $W = 50$.

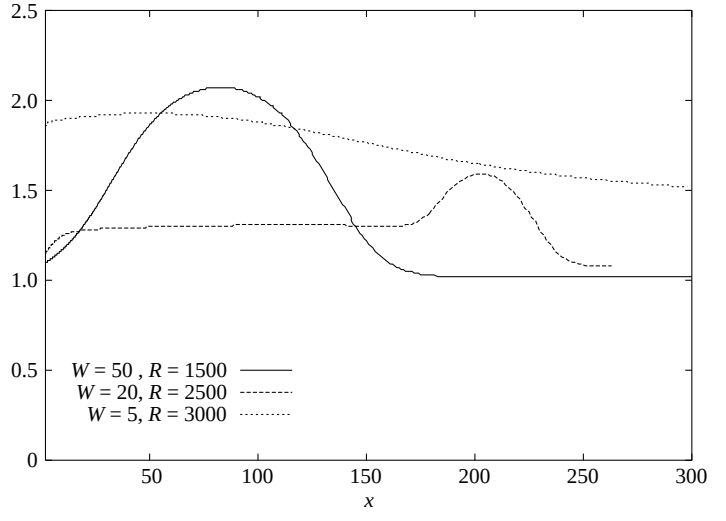

FIGURE 21. Edge velocity (at $y = W/2$) from the Navier–Stokes computations for $R = 3000$, $W = 5$; $R = 2500$, $W = 20$; $R = 1500$, $W = 50$.

the eddy is predominantly linear, becoming uniform outside the eddy region. The type III solutions figure 24 show that after reattachment, the velocity recovers, becoming positive and tending to a uniform state with increasing x.

Finally, one other point concerning the boundary layer theory is that in both Smith (1985*a*) and Milos & Acrivos (1986) numerical difficulties were encountered in the limit of the eddy width parameter λ approaching zero. The solutions of Milos & Acrivos (1986) suggest the appearance of a singularity as λ approaches zero. Without more detailed evidence and analysis it is difficult to make any substantive comparisons, but it is possible that a singularity may point to the disappearance of the boundary

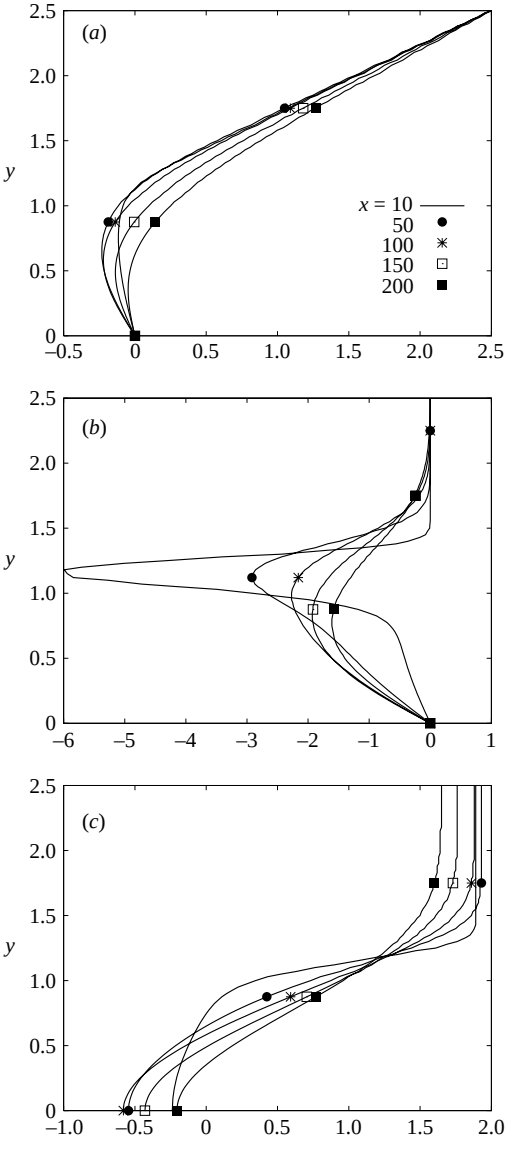

FIGURE 22. Graphs of (*a*) streamfunction, (*b*) vorticity, and (*c*) streamwise velocity at various x locations for $W = 5$, $R = 3000$.

layer type of solution and the appearance of the type III solution. What is also clear is that type II solutions do not seem to be described by the boundary layer theory.

Therefore although the Navier–Stokes computations are qualitatively in line with the theory, a more detailed and more accurate solution of the boundary layer problem is needed before any substantive claims can be made.

7. Conclusion

We have used a spectral Chebychev collocation combined with a high-order finite difference numerical method to compute the solution for flow past a cascade of

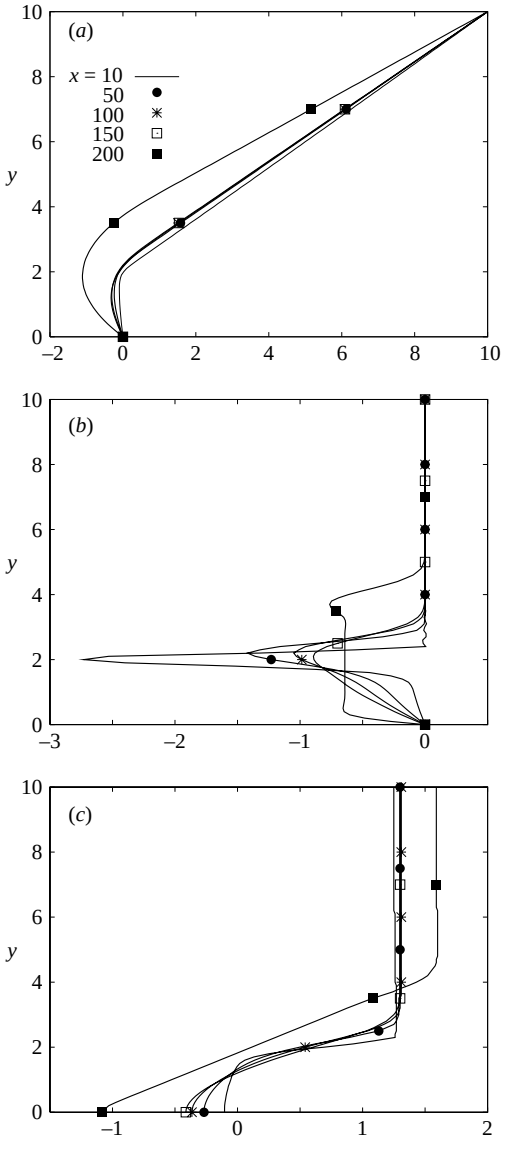

FIGURE 23. Graphs of (*a*) streamfunction, (*b*) vorticity, and (*c*) streamwise velocity at various x locations for $W = 20$, $R = 2500$.

cylinders for $R \gg 1$. Excellent agreement has been found for small gap widths with previous work by Fornberg (1991). For large gap widths, and increasing Reynolds numbers there are some differences between our results and those of Fornberg (1991). The reasons for the differences are not clear although it is suggested here that they may be due to the higher-order accuracy of the method used here. It is possible that the differences may be due to inadequately resolved numerical computations. It is argued that the small gap width results results presented here are fully resolved.

Our results compare well with theoretical estimates of certain global properties, especially for small gap widths. However it has been pointed out that the eddy

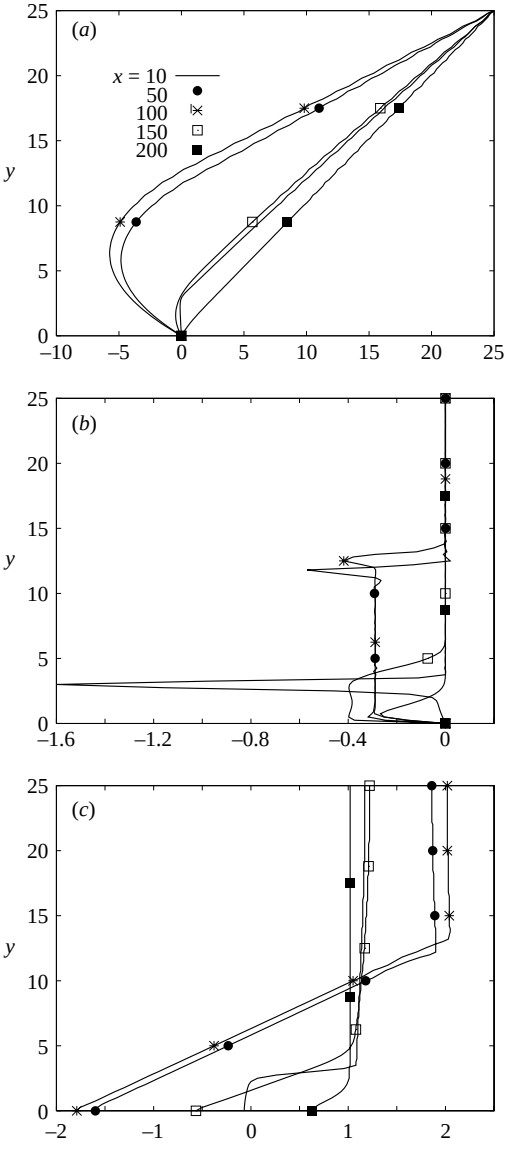

FIGURE 24. Graphs of (*a*) streamfunction, (*b*) vorticity, and (*c*) streamwise velocity at various x locations for $W = 50$, $R = 1500$.

properties for small gap widths are qualitatively more similar to those for a boundary-layer solution than those stemming from a limit of the potential vortex model. In particular the latter has constant eddy vorticity which is inconsistent with the numerical results presented here and elsewhere. Thus the good comparisons obtained between the theoretical estimates and numerical results requires further examination.

Castro (2002) has managed to compute to large values of the Reynolds numbers flow for a cascade of flat plates in a stratified fluid, and qualitatively the results reported there are very similar to those here in terms of the development of the eddy features for varying gap widths.

J.S.B.G. would like to thank Professors Chernyshenko, Castro and Smith for helpful discussion related to their work on this and related problems. The referees are also thanked for their helpful comments.

REFERENCES

Acrivos, A., Leal, L., Snowden, D. & Pan, F. 1968 Further experiments on steady separated flow past bluff objects. *J. Fluid Mech.* **34**, 25–48.

Acrivos, A., Snowden, D., Grove, A. & Petersen, E. 1965 The steady flow past a circular cylinder at large Reynolds numbers. *J. Fluid Mech.* **21**, 737–760.

Azzam, N. 2003 Numerical solution of the navier-stokes equations for the flow in lid-driven cavity and a cylinder cascade PhD thesis, University of Manchester (submitted).

Batchelor, G. 1956 A proposal concerning laminar wakes behind bluff bodies at large Reynolds numbers. *J. Fluid Mech.* **1**, 177–190.

Bhattacharya, S., Dennis, S. & Smith, F. 2001 Separating flow past a surface-mounted blunt obstacle. *J. Engng Maths* **39**, 47–62.

Canuto, C., Hussaini, M. Y., Quaternoni, A. & Zang, T. 1987 *Spectral Methods in Fluid Dynamics.* Springer.

Castro, I. 2002 Weakly stratified laminar flow past normal flat plates. *J. Fluid Mech.* **454**, 21–46 .

Chernyshenko, S. 1988 The asymptotic form of the stationary separated circumference of a body at high Reynolds numbers. *Prikl. Matem. Mekh.* **52**, 958–966.

Chernyshenko, S. 1993 Stratified flow in a channel. *J. Fluid Mech.* **250**, 423–431.

Chernyshenko, S. 1998 Asymptotic theory of global separation. *Appl. Mech. Rev.* **51**, 523–535.

Chernyshenko, S. & Castro, I. 1993 High-Reynolds number asymptotics of the steady flow through a row of bluff bodies. *J. Fluid Mech.* **257**, 421–449.

Chernyshenko, S. & Castro, I. 1996 High Reynolds number weakly stratified flow past an obstacle. *J. Fluid Mech.* **317**, 155–178.

Davies, C. & Carpenter, P. 1997 Numerical simulation of the evolution of Tollmien-Schlichting waves over finite compliant panels. *J. Fluid Mech.* **352**, 205–243.

Ehrenstein, E. & Peyret, R. 1989 A chebychev collocation method for the Navier–Stokes equations with application to double-diffusive convection. *Intl J. Numer. Meth. Fluids* **9**, 427–452.

Fornberg, B. 1980 A numerical study of steady viscous flow past a circular cylinder. *Intl J. Numer. Meth. Fluids* **98**, 819–855.

Fornberg, B. 1983 Steady viscous flow past a circular cylinder. *NASA Conf Publ* 2295, pp. 201–224.

Fornberg, B. 1985 Steady viscous flow past a cicular cylinder up to Reynolds number 600. *J. Comput. Phys.* **61**, 297–320.

Fornberg, B. 1991 Steady incompressible flow past a row of circular cylinders. *J. Fluid Mech.* **225**, 655–671.

Fornberg, B. 1998 *A Practical Guide to Pseudospectral Methods.* Cambridge University Press.

Ingham, D., Tang, T. & Morton, B. 1990 Steady two-dimensional flow through a row of normal flat plates. *J. Fluid Mech.* **210**, 281–302.

Kirchoff, G. 1869 Zur theorie freier-flussigkeits strahlen. *J. Reine Angew Math Bd* **70**(H4), 289–298.

Milos, F. & Acrivos, A. 1986 Steady flow past sudden expansions at large Reynolds numbers Part i. Boundary layer solutions. *Phys. Fluids* **29**, 1353–1359.

Milos, F. & Acrivos, A. 1987 Steady flow past sudden expansions at large Reynolds numbers. Part ii. Navier–Stokes solutions for the cascade expansion. *Phys. Fluids* **30**, 7–18.

Natarajan, R., Fornberg, B. & Acrivos, A. 1993 Flow past a row of flat plates at large Reynolds numbers. *Proc. R. Soc. Lond.* A **441**, 211–235.

Peregrine, H. 1985 A note on the steady high Reynolds number flow past a circular cylinder. *J. Fluid Mech.* **157**, 493–500.

Sadovskii, V. 1970 A region of uniform vorticity in plane potential flow. *Uch. Zap. TsAGI* **1** (4), 1–9.

Sadovskii, V. 1971 On local properties of vortex flows. *Uch. Zap. TsAGI* **3** (4), 117–120.

Smith, F. 1979 Laminar flow of an incompressible fluid past a bluff body: The separation, reattachment, eddy properties and drag. *J. Fluid Mech.* **92**, 171–205.

Smith, F. 1985*a* On large-scale eddy closure. *J. Math. Phys. Sci.* **19**, 1–80.

Smith, F. 1985*b* A structure for laminar flow past a bluff body at large Reynolds numbers. *J. Fluid Mech.* **155**, 175–191.

Sychev, V. 1967 On steady laminar flow behind a bluff body at high Reynolds numbers. In *Proc. 8th Symposium on Current Problems of the Mechanics of Liquids and Gases. Tarda, Poland.*

Sychev, V. 1982 Asymptotic theory of separated flows. *Izv. AN SSSR, Mekh Zhidki* **2**, 20–30.

Taganov 1968 Contribution to the theory of stationary separation zones. *Izv. AN SSSR Mekh Zhidk i Gaza* **5**, 3–19.